Published in final edited form as:

Nat Chem Biol. 2020 September ; 16(9): 979–987. doi:10.1038/s41589-020-0550-9.

Identification of a potent and selective covalent Pin1 inhibitor

Benika J. Pinch[1,2,3], **Zainab M. Doctor**[2,3,10], **Behnam Nabet**[2,3,10], **Christopher M. Browne**[2,3,9], **Hyuk-Soo Seo**[2,3], **Mikaela L. Mohardt**[2], **Shingo Kozono**[4], **Xiaolan Lian**[4], **Theresa D. Manz**[2,3,5], **Yujin Chun**[3], **Shin Kibe**[4], **Daniel Zaidman**[6], **Dina Daitchman**[6], **Zoe C. Yeoh**[2,3], **Nicholas E. Vangos**[2,3], **Ezekiel A. Geffken**[2,3], **Li Tan**[2], **Scott B. Ficarro**[2,7], **Nir London**[6], **Jarrod A. Marto**[7,8], **Stephen Buratowski**[3], **Sirano Dhe-Paganon**[2,3], **Xiao Zhen Zhou**[4], **Kun Ping Lu**[4], **Nathanael S. Gray**[2,3]

[1]Department of Chemistry and Chemical Biology, Harvard University, Cambridge, Massachusetts

[2]Department of Cancer Biology, Dana-Farber Cancer Institute, Boston, Massachusetts

[3]Department of Biological Chemistry and Molecular Pharmacology, Harvard Medical School, Boston, Massachusetts

[4]Division of Translational Therapeutics, Department of Medicine and Cancer Research Institute, Beth Israel Deaconess Medical Center Harvard Medical School, Boston, Massachusetts

[5]Department of Pharmacological and Medicinal Chemistry, Saarland University, Saarbruecken, Germany

[6]Department of Organic Chemistry, Weizmann Institute of Science, Rehovot, Israel

[7]Blais Proteomics Center, Dana-Farber Cancer Institute, Boston, Massachusetts

[8]Department of Pathology, Brigham and Women's Hospital and Harvard Medical School, Boston, Massachusetts

[9]Present address: Discovery Biology, Discovery Sciences, Biopharmaceuticals R&D, AstraZeneca, Boston, MA USA

[10]Equal contribution

Abstract

Peptidyl-prolyl *cis*/*trans* isomerase NIMA-interacting 1 (Pin1) is commonly overexpressed in human cancers, including pancreatic ductal adenocarcinoma (PDAC). While Pin1 is dispensable for viability in mice, it is required for activated Ras to induce tumorigenesis, suggesting a role for

Correspondence may be addressed to: Nathanael S. Gray (Nathanael_Gray@dfci.harvard.edu) Kun Ping Lu (klu@bidmc.harvard.edu).

AUTHOR CONTRIBUTIONS

B.J.P. performed the chemical synthesis, biological characterization, and wrote the manuscript. Z.M.D. generated cell lines, performed the GFP dropout experiment and RNAseq analysis. B.N. generated cell lines and designed and supervised biological studies. C.M.B., S.B.F., and J.A.M. performed CITe-Id and mass spectrometry studies. M.L.M. assisted in Pin1 mutant cellular studies. S. Kozono, S. Kibe, and X.L. performed the FP assay. D.Z, D.D, and N.L. provided computational docking support. L.T. advised on compound design and T.D.M. provided support for the chemical synthesis and biological characterization. Z.C.Y., N.E.V, E.A.G., and H.-S.S. performed the protein expression and crystallography, H.-S.S and S.D.-P. analyzed the crystallography data. Y.C. and S.B. performed the yeast complementation experiments and analysis. K.P.L and X.Z.Z. helped supervise the project and provided experimental support. N.S.G conceived of and led this study.

Pin1 inhibitors in Ras-driven tumors, such as PDAC. We report the development of rationally designed peptide inhibitors that covalently target Cys113, a highly conserved cysteine located in the Pin1 active site. The inhibitors were iteratively optimized for potency, selectivity, and cell permeability to give BJP-06–005-3, a versatile tool compound with which to probe Pin1 biology and interrogate its role in cancer. In parallel to inhibitor development, we employed genetic and chemical-genetic strategies to assess the consequences of Pin1 loss in human PDAC cell lines. We demonstrate that Pin1 cooperates with mutant KRAS to promote transformation in PDAC, and that Pin1 inhibition impairs cell viability over time in PDAC cell lines.

INTRODUCTION

Proline-directed phosphorylation controls numerous cellular processes, including cell cycle progression, transcription, and differentiation. Proline (Pro) is unique among the amino acids in that its imidic peptide bond can populate either the *cis* or the *trans* conformation[1,2] and the intrinsic isomerization rate of Pro-containing motifs is slow relative to biological signaling, requiring catalysis by peptidyl-prolyl isomerases (PPIases). As the only known phosphorylation-dependent PPIase, Pin1 acts in tandem with Pro-directed kinases and phosphatases, which are conformation-specific, to control the stability, localization, and activity of their common targets[3].

Pin1 is frequently overexpressed in cancer[4], including pancreatic ductal adenocarcinoma (PDAC), and Pin1 overexpression correlates with poor prognosis[5]. Pin1 ablation is reported to prevent MMTV-Ras-driven mouse mammary gland carcinoma, indicating that Pin1 is a key effector in Ras signaling[6]. While mutations in *KRAS* are observed in 90–95% of PDAC cases[7], it has historically proven difficult to develop inhibitors of mutant KRAS, spurring efforts to target proteins that facilitate Ras-mediated transformation, such as Pin1. Notably, while the yeast homolog of Pin1 (Ess1) is essential[8], Pin1-null mice develop normally, though with decreased body weight[9], suggesting that Pin1 inhibition could reduce tumorigenic potential with limited toxicity.

Several Pin1 inhibitors have been described to date, including juglone[10], all-trans retinoic acid (ATRA)[11], arsenic trioxide (ATO)[12], KPT-6566[13], and (*S*)-2[14]. However, these compounds lack the potency and/or selectivity to accurately assess Pin1-mediated phenotypes[15]. Notably, while reported Pin1 inhibitors demonstrate potent cellular cytotoxicity, Pin1 was not identified as a cancer dependency in genome-wide CRISPR screens conducted across hundreds of cancer cell lines (Cancer Dependency Map) – thus highlighting a contradiction in our understanding of Pin1 biology. A selective, potent and cell permeable Pin1 inhibitor is required to effectively evaluate the role of Pin1 in oncogenesis.

Targeted covalent inhibitors allow for improved potency and selectivity, and prolonged duration of action[16,17]. Oxidation of the conserved cysteine in the Pin1 active site, Cys113, eliminates its isomerase activity and impairs its cellular function[18], suggesting that covalent binders would irreversibly inhibit Pin1. Also, previously reported inhibitors juglone[10], KPT-6566[13], and (*S*)-2[14] provide precedent for targeting Pin1 covalently.

In this study, we describe the structure-guided design of covalent peptides targeting Pin1 Cys113 by modifying the high affinity but cell-impermeable substrate mimetic inhibitor, D-PEPTIDE[19]. We demonstrate that the resulting inhibitor, BJP-06–005-3 (**1**), is potent, cell-permeable, and highly selective. We further show that Pin1 cooperates with $KRAS^{G12V}$ to promote cellular transformation. By leveraging covalent Pin1 inhibition, as well as targeted Pin1 degradation using the degradation tag (dTAG) strategy[20], we demonstrate that Pin1 loss impairs cell growth and transformation in PDAC model systems. Ultimately, this work showcases a set of robust chemical, genetic, and chemical-genetic tools with which to study the role of Pin1 in oncogenesis.

RESULTS

Structure-guided design of Pin1 inhibitors

To develop a Pin1-targeted probe, we modified D-PEPTIDE (Ac-Phe-D-pThr-Pip-Nal-Gln-NH_2; K_i = 20 nM), which is a potent Pin1 inhibitor that cannot enter cells[19]. We sought to replace the phosphate of D-PEPTIDE with a cell-permeable moiety, while compensating for any resulting loss in potency with a covalent bond to Cys113. Based on the Pin1/ D-PEPTIDE co-crystal structure (PDB 2ITK)[19], the N-terminus of D-PEPTIDE provided the best access to Cys113 and therefore served as the attachment site for a cysteine-targeting electrophile (Fig. 1a–b). We chose an α-chloroacetamide as the electrophile based on a prior proteome-wide screen to quantify cysteine reactivity, which identified several α-chloroacetamide-containing fragments that labeled Pin1[21]. An α-chloroacetamide is also featured in KPT-6566[13].

We profiled each newly synthesized inhibitor in a fluorescence polarization (FP) assay[11] following a 12 h incubation of the inhibitor with recombinant Pin1 to allow sufficient time for covalent labeling. Given precedent that a carboxylate can successfully replace a phosphate in Pin1 inhibitors[22], we initially substituted the phospho-Thr of D-PEPTIDE with a carboxylic acid. While an Asp-containing derivative (**2**) did not bind Pin1, the extra methylene of a Glu enabled Pin1 binding with an apparent K_i of 2 μM (**3**). Replacing the Gln with Arg improved potency by 12-fold to give BJP-02–118-2 (**4**). We obtained a co-crystal structure of BJP-02–118-2 bound to Pin1, which revealed a charge-charge interaction with Pin1 Glu135 (PDB 6O33; Supplementary Table 1). We then further enhanced potency by substituting the Arg with citrulline (Cit) (**5**) and the naphthylalanine (Nal) with Trp, improving the apparent K_i to 30 nM (**6**) (Supplementary Fig. 1a–c).

Despite having successfully replaced the phosphate with a carboxylate, the resulting inhibitors had negative cLogP values and low lipophilicity, which governs passive membrane permeability[23] (Supplementary Fig. 1d). We therefore increased lipophilicity by capping the C-terminus with an ethyl ester, methylating the N-terminal nitrogen to eliminate a hydrogen bond donor, and replacing the Glu with Phe to give BJP-06–005-3, with an apparent K_i of 15 nM (Fig. 1c–d). We hypothesized that the surprising affinity of BJP-06–005-3 might be explained by a cation-pi interaction between the Phe benzene and Arg68 or Arg69 in the Pin1 phosphate-binding pocket. Notably, while D-PEPTIDE features a D-phos.Thr residue, the covalent binding of BJP-06–005-3 flips the preferred stereochemistry at that position such that a D-Phe substitution (**7**) eliminates Pin1 binding (Supplementary Fig. 2a–b).

We next explored whether alternate thiol-targeting electrophiles were tolerated by substituting the α-chloroacetamide with an acrylamide (**8**), α-fluoroacetamide (**9**), epoxide (**10**), or 2-chloropropionamide (**11**). For these studies, we used a derivative of BJP-06–005-3 lacking the methylated N-terminal nitrogen (**12**, apparent K_i = 7.4 nM). As a control, we also synthesized the unreactive *N*-methylacetamide (**13**) (Fig. 1e). None of the compounds featuring alternate electrophiles bound Pin1, highlighting that the α-chloroacetamide is necessary to achieve covalency (Supplementary Fig. 2c). Similarly, an analog of BJP-06–005-3 in which the α-chloroacetamide was replaced with an *N*-methylacetamide (BJP-R (**14**), Supplementary Fig. 2a–b) lost all binding to Pin1 indicating that, despite optimizing the noncovalent interactions, the binding of BJP-06–005-3 is primarily driven by its covalency. BJP-R was subsequently used as a negative control compound. In summary, by making a series of structure-guided modifications to D-PEPTIDE and leveraging a covalent binding mode, we developed BJP-06–005-3 as a high affinity Pin1 binder.

BJP-06–005-3 is a potent and covalent Pin1 inhibitor

We next evaluated the inhibitory activity, covalency, and binding mode of BJP-06–005-3 (Supplementary Fig. 3a). We assessed the ability of BJP-06–005-3 to inhibit Pin1 enzymatic activity using a chymotrypsin-coupled peptidyl-prolyl isomerization assay (PPIase assay). In this spectrophotometric assay, the peptidic substrate (Succ-Ala-p.Ser-Pro-Phe-pNA) is only cleaved by chymotrypsin when the peptidyl-prolyl bond is in the *trans* conformation[11]. BJP-06–005-3 potently inhibited Pin1 catalytic activity with an apparent K_i of 48 nM (Fig. 2a). Next, to assess the covalency of BJP-06–005-3, recombinant full-length Pin1 protein was analyzed by intact mass spectrometry following incubation with BJP-06–005-3 or DMSO. BJP-06–005-3 showed 100% covalent labeling of Pin1 as indicated by a 702 Da molecular weight increase, corresponding to modification of Pin1 by BJP-06–005-3 upon loss of its chloride (Fig. 2b). Trypsin digest confirmed the site of covalent modification as Cys113 (Supplementary Fig. 3b). We next performed the FP assay in a dose- and time-dependent manner (0–30 min) to assess the k_{inact}/K_i of BJP-06–005-3, in which K_i describes the reversible binding and k_{inact} the maximum rate of inactivation[24]. We determined the k_{inact} to be 0.08 ± 0.01 min^{-1} and the K_i to be 1800 ± 670 nM (k_{inact}/K_i = 740 $M^{-1}s^{-1}$) (Supplementary Fig. 3c). The apparent K_i of BJP-06–005-3 decreases with increasing incubation time, reaching 15 nM following a 12 h incubation with Pin1.

To evaluate the binding mode of BJP-06–005-3 we sought to obtain a co-crystal structure with Pin1. Unfortunately, BJP-06–005-3 precipitated out of the crystallization buffer, prompting us to synthesize a more hydrophilic and water soluble derivative of BJP-06–005-3 by replacing its C-terminal ethyl ester with an amide to give BJP-07–017-3 (**15**), with an apparent K_i of 15 nM (Fig. 2c, Supplementary Fig. 3d). This enabled us to obtain a 1.6 Å co-crystal structure of BJP-07–017-3 bound to full-length Pin1 (PDB 6O34), which showed good ligand occupancy and clear electron density to Cys113, consistent with covalent modification (Supplementary Fig. 3e, Supplementary Table 1). In this structure, the pipecolinic acid (Pip) of BJP-07–017-3 acts as a proline mimetic, making hydrophobic contacts with Leu122, Met130, Phe134, His59, and His157 in the prolyl-binding pocket. The Cit of BJP-07–017-3 is engaged in hydrogen bonds to the backbone amides of Met130 and Glu135, while the Trp interacts with the sidechain of Met130 in a methionine-aromatic

motif[25] (Fig. 2d). Given that both Arg68 and Arg69 were disordered, we were unable to conclude whether the Phe of BJP-07–017-3 is engaged in a cation-pi interaction, as per our original hypothesis. Collectively, these biochemical and structural data confirmed that BJP-06–005-3 is a potent and covalent Pin1 inhibitor.

BJP-06–005-3 is selective and engages cellular Pin1

To evaluate the selectivity of BJP-06–005-3 and its ability to covalently modify Pin1 in cells, we synthesized a desthiobiotin (DTB)-labeled derivative (BJP-DTB, **16**), which retained high affinity for Pin1 (Supplementary Fig. 4a–b). BJP-DTB exhibited potent and rapid pull-down of Pin1 from PATU-8988T cell lysates (Supplementary Fig. 4c–d), and pull-down was selectively outcompeted following pre-incubation with BJP-06–005-3 (Supplementary Fig. 4e). In addition, BJP-DTB pulled-down WT Pin1 but not a C113S Pin1 mutant, validating its covalent binding mode (Supplementary Fig. 4f).

We employed BJP-DTB to assess the selectivity of BJP-06–005-3 using Covalent Inhibitor Target Site Identification (CITe-Id), which quantifies the proteome-wide binding of covalent inhibitors to individual cysteines[26]. In this competition assay, HEK293 lysates were preincubated with BJP-06–005-3, followed by co-incubation with BJP-DTB (Fig. 3a). Across the proteome, out of 604 sites reproducibly labeled by BJP-DTB in two independent experiments, Pin1's Cys113 was the only cysteine that exhibited dose-dependent binding to BJP-06–005-3 (Fig. 3b; Supplementary Dataset 1), highlighting the remarkable selectivity of this inhibitor.

To assess the permeability and cellular target engagement of BJP-06–005-3, we performed a live cell competition assay (Supplementary Fig. 5a). Following a 5 h treatment in PATU-8988T cells, BJP-06–005-3 exhibited dose-dependent competition with BJP-DTB for binding to Pin1, with maximal engagement observed at 10 μM, while the negative control, BJP-R, did not show competition (Fig. 3c). Engagement of Pin1 by BJP-06–005-3 was evident within 4 h (Fig. 3d) and was maintained for 48 h following a single treatment. Pin1 engagement was lost by 72 h, likely due to hydrolysis of the peptide (Supplementary Fig. 5b–d). BJP-06–005-3 similarly outcompeted BJP-DTB in PC3 (prostate cancer) and MDA-MB-468 (breast cancer) cells, with slight loss of Pin1 engagement observed 48 h after treatment (Supplementary Fig. 5e). These data suggest that BJP-06–005-3 engages Pin1 for 48 h following a single 5–10 μM treatment across multiple cancer cell types. However, while BJP-06–005-3 exhibits strong cellular target engagement, it has poor mouse liver microsome stability ($T_{1/2}$ = 1.2 mins), limiting its applications to biochemical and cell-based assays.

Covalent inhibitors can induce degradation of their target proteins, often by causing structural rearrangement[27]. Pin1 is frequently degraded following inhibitor binding, as previously demonstrated with ATRA[11], ATO[12], and KPT-6566[13]. Similarly, BJP-06–005-3 caused partial Pin1 degradation following a 48 h treatment in two $KRAS^{G12V}$ PDAC cell lines, PATU-8988T and PATU-8902, and BJP-06–005-3 reduced Pin1 half-life in PATU-8988T cells (Supplementary Fig. 6a–d). However, this phenotype was cell line-dependent as BJP-06–005-3 did not degrade Pin1 across a panel of additional cancer cell lines. In all cell lines tested, however, binding of BJP-06–005-3 to Pin1 caused an upward shift in the Pin1 protein band by immunoblot, corresponding to the molecular weight

increase when Pin1 (~18 kDa) is labeled by BJP-06–005-3 (MW 702) (Supplementary Fig. 6d). Taken together, these findings affirmed that BJP-06–005-3 is selective and engages cellular Pin1.

Pin1 cooperates with KRAS^{G12V} to promote transformation

Prior evidence suggests that Pin1 is required for Ras-induced transformation[6], and Pin1 overexpression in Ras-transformed human mammary epithelial cells is reported to increase tumor incidence in mice[28]. We sought to evaluate whether Pin1 cooperates with mutant KRAS to coordinate cell transformation, and to investigate the role of Pin1 in PDAC, a mutant KRAS-driven cancer. To assess the effects of Pin1 overexpression on transformation, we transduced NIH/3T3 cells with doxycycline (Dox)-inducible Pin1 alone, or in combination with FKBP12^{F36V}-KRAS^{G12V}, which is a functional oncoprotein[20]. After confirming that Dox treatment for 48 h effectively increased Pin1 levels (Fig. 4a), we assessed the ability of both cell lines to form three-dimensional (3D)-spheroid suspensions in ultra-low adherent (ULA) conditions to assay cellular transformation[29,30]. Compared to parental NIH/3T3 cells, Pin1 overexpression led to a modest increase in spheroid formation, which was more significant in the context of FKBP12^{F36V}-KRAS^{G12V} expression (Fig. 4b), though this trend was less pronounced in two-dimensional (2D) adherent monolayers (Fig. 4c). These results demonstrate that Pin1 overexpression is mildly transformative by itself, and cooperates with activated KRAS to increase transformation.

Using genetic strategies, we assessed the effects of Pin1 loss on viability in a PDAC context, laying the groundwork for subsequent studies with BJP-06–005-3. We performed a competition-based CRISPR/Cas9 GFP dropout assay[31,32] in Cas9-expressing PATU-8988T cells (Fig 4d), using eight GFP-tagged sgRNAs targeting *PIN1*, which were confirmed to induce Pin1 knockout (KO) (Supplementary Fig. 6e, Supplementary Table 2–3). By monitoring the GFP signal over time, we found that Pin1 KO led to mild but statistically significant, time-dependent defects in PDAC cell growth (Fig. 4d; Supplementary Table 4).

To confirm this observation, we isolated single cell Pin1$^{-/-}$ clones from PATU-8988T cells and compared the basal growth rate of a clone lacking Pin1 (referred to as C2) to a clone that maintained expression of endogenous Pin1 (referred to as C1) (Fig. 4e). C2 exhibited a significantly slower growth rate, as compared to parental PATU-8988T cells or C1 (Fig. 4f). To evaluate whether Pin1's substrate-binding WW domain, and/or its catalytic PPIase domain were required for this viability effect, we transduced C2 with WT Pin1, a Pin1 mutant lacking WW domain activity (W34A), or Pin1 mutants with disrupted PPIase activity (K63A; C113S)[33] (Fig. 4g). While expression of WT Pin1 increased the basal growth rate of C2, expression of any of the Pin1 mutants did not alter the basal growth rate (Fig. 4h), suggesting that Pin1 must have functional WW and PPIase domains to mediate enhanced cell viability in PATU-8988T cells. Collectively, these data indicate that Pin1 overexpression cooperate with KRAS^{G12V} to enhance cell transformation, and that Pin1 KO causes viability defects in PATU-8988T cells. This supports the further evaluation of BJP-06–005-3 in PDAC cellular contexts.

BJP-06–005-3 has Pin1-dependent cell viability effects

We next assessed the effects of BJP-06–005-3 on cell viability. While BJP-06–005-3 treatment was largely non-toxic following a 4-day treatment in PATU-8988T cells, increasing the duration of the experiment to 8-days led to diminished cell viability, with replenishment of BJP-06–005-3 every 48 h to ensure durable target engagement. The negative control, BJP-R, did not affect viability (Supplementary Fig. 7a). Across a panel of cancer cell lines, BJP-06–005-3 consistently reduced cell viability in a dose- and time-dependent manner (Supplementary Fig. 7b–g).

To confirm that these antiproliferative effects were Pin1-mediated, we compared the effects of BJP-06–005-3 in C1 (Pin1 WT) versus C2 (Pin1 KO). BJP-06–005-3 led to a dose- and time-dependent decrease in cell growth in C1, while it did not affect proliferation in C2 (Fig. 5a). We next transduced C2 with Dox-inducible Pin1 (Supplementary Fig. 7h), and found the resulting cells to be re-sensitized to BJP-06–005-3 in the presence of Dox (Fig. 5b). Furthermore, BJP-06–005-3 impacted viability in 3D-spheroids after a 4-day treatment in PATU-8988T parental cells, but not in C2, suggesting a Pin1-mediated effect on cell transformation (Fig. 5c). By contrast, the previously reported covalent Pin1 inhibitors, juglone[10] and KPT-6566[13], induced identical anti-proliferative effects in C1 and C2, indicating that their viability effects are likely mediated by off-targets. We were also unable to validate that KPT-6566 engages cellular Pin1 using our BJP-DTB competition assay (Supplementary Fig. 8a–d).

To complement the characterization of BJP-06–005-3, we employed our dTAG system, in which a heterobifunctional degrader (dTAG-13) co-opts cereblon to rapidly and selectively degrade $FKBP12^{F36V}$-tagged fusions[20]. To first establish that N-terminally tagged Pin1 ($FKBP12^{F36V}$-Pin1) was functional, we performed complementation experiments in Saccharomyces cerevisiae, in which the *PIN1* homolog, *ESS1*, is an essential gene[8]. Overexpression of Pin1 or $FKBP12^{F36V}$-Pin1 successfully supported growth of an *ESS1* deletion strain, and immunoblotting confirmed expression of the fusion protein (Supplementary Fig. 9a–b).

To implement the dTAG system in PDAC cells, we exogenously expressed $FKBP12^{F36V}$-Pin1 in C2 (referred to as C2 + $FKBP12^{F36V}$-Pin1) (Supplementary Fig. 9c). Treatment with dTAG-13 caused rapid and potent degradation of $FKBP12^{F36V}$-Pin1, with maximal degradation at 100–500 nM, and with the hook effect[34] apparent by 1 μM, at which the binary complexes outcompete formation of a productive ternary complex (Supplementary Fig. 9d–e). $FKBP12^{F36V}$-Pin1 degradation occurred within 2–4 h (Fig. 5d), and degradation was rescued upon pretreatment with carfilzomib (proteasome inhibitor) or MLN4924 (NEDD8-activating enzyme inhibitor), confirming a proteasome- and neddylation-dependent mechanism (Supplementary Fig. 9f).

Introduction of $FKBP12^{F36V}$-Pin1 into C2 restored the growth rate to parental levels (Fig. 5e), and prolonged $FKBP12^{F36V}$-Pin1 degradation diminished cell proliferation after 6–8 days. This phenotype was apparent upon treatment with 100 or 500 nM dTAG-13, but not at 2.5 μM, consistent with the appearance of the hook effect at higher doses (Supplementary Fig. 9g). Furthermore, while C2 was resistant to BJP-06–005-3, treatment with BJP-06–

005-3 in FKBP12^{F36V}-Pin1-expressing C2 restored the time-dependent anti-proliferative effects (Fig. 5f). FKBP12^{F36V}-Pin1 could also be pulled down by BJP-DTB, which was outcompeted upon BJP-06–005-3 pre-treatment (Supplementary Fig. 9h). The effects of FKBP12^{F36V}-Pin1 degradation were therefore consistent with BJP-06–005-3 treatment, further validating our inhibitor's on-target pharmacology.

Cell cycle and transcriptional effects of BJP-06–005-3

We next explored whether the time-dependent viability effects upon Pin1 loss or inhibition might be explained by subtle changes in cell cycle progression, which can translate to exponential changes in cell number over time[35]. Given that Pin1 regulates the G2/M transition through its interaction with mitotic proteins, including Cdc25C and Wee1[3], we hypothesized that Pin1 might impact phosphorylation of CDK1 Tyr15, a critical regulator of mitotic entry and a downstream target of Wee1. In a previous study, depletion of Pin1-binding proteins from *Xenopus* egg extracts resulted in hyperphosphorylation of Cdc2[36]. We found that phospho-CDK1 Tyr15 was elevated in C2 as compared to C1 (Fig. 6a). Similarly, BJP-06–005-3 increased phospho-CDK1 Tyr15 in C1 (Fig. 6b), but not in C2 (Supplementary Fig. 10a). dTAG-13-mediated degradation of FKBP12^{F36V}-Pin1 also increased phospho-CDK1 Tyr15 (Supplementary Fig. 10b).

To evaluate the cell cycle effects of Pin1 inhibition, we performed propidium iodide staining in PATU-8988T cells treated with BJP-06–005-3 for 4–48 h. At all time points tested, BJP-06–005-3 modestly decreased G2/M (statistically insignificant, Bonferroni-corrected two-way ANOVA) and increased G1 phase cells (adj. $p < 0.05$ at all time points, Bonferroni-corrected two-way ANOVA). Similarly, degradation of FKBP12^{F36V}-Pin1 moderately decreased G2/M cells (adj. $p = 0.0435$, Bonferroni-corrected two-way ANOVA) and increased G1 cells (adj. $p = 0.0071$, Bonferroni-corrected two-way ANOVA) (Supplementary Fig. 10c–e).

To further explore the downstream consequences of Pin1 inhibition, we evaluated the effects of BJP-06–005-3 on reported Pin1 substrates, including β-Catenin[37], NFkB p65[38], and c-Myc[39]. We observed no change in the expression of β-Catenin or p65 upon BJP-06–005-3 treatment (Fig. 6b), which could be explained by low basal activation of Wnt/β-Catenin and NFkB signaling in PATU-8988T cells. Furthermore, following recombinant Wnt3a treatment to increase nuclear β-Catenin, BJP-06–005-3 did not affect expression or nuclear/cytoplasmic localization of β-Catenin (Supplementary Fig. 10f–h). However, in accordance with literature precedent that Pin1 enhances c-Myc turnover[39], BJP-06–005-3 treatment increased c-Myc protein levels (Fig. 6b), as did dTAG-13-mediated FKBP12^{F36V}-Pin1 degradation (Supplementary Fig. 10b).

To broadly profile the downstream changes upon covalent Pin1 inhibition, we assessed the transcriptional consequences of BJP-06–005-3 in PATU-8988T cells. We identified 3220 significantly differentially expressed transcripts (2587 up- and 633 down-regulated at 1.25-fold; $p < 0.05$) following a 4 h treatment with BJP-06–005-3, normalized relative to DMSO and BJP-R (Supplementary Dataset 2; Supplementary Fig. 11a). Gene Set Enrichment Analysis (GSEA) revealed enrichment of several pathways in the differentially expressed transcripts, including GPCR ligand signaling, extracellular matrix organization, and integrin

cell surface interactions (Supplementary Fig. 11b–f). EnrichR[40] analysis of the differentially expressed genes to identify the transcription factors that might be coordinating these changes identified Myc target genes as amongst the most enriched sets, suggesting that the transcriptional responses to BJP-06–005-3 may occur through reduction of Myc transcriptional activity (Supplementary Fig. 11g). This is consistent with literature reports that Pin1 enhances c-Myc DNA binding and oncogenic activity[41], and our observations of increased c-Myc turnover.

Given the critical role of Myc in Ras-driven cancer growth[42], we hypothesized that Pin1 inhibition may cooperate with KRAS loss. We assessed whether the anti-proliferative effects of FKBP12^{F36V}-KRAS^{G12V} degradation[43] could be amplified by BJP-06–005-3. We used a PATU-8988T FKBP12^{F36V}-KRAS^{G12V}; *KRAS*$^{-/-}$ clone in which dTAG-13 treatment degrades FKBP12^{F36V}-KRAS^{G12V}, leading to modest changes in cell proliferation[43]. We confirmed that dTAG-13 treatment degraded FKBP12^{F36V}-KRAS^{G12V}, which was unchanged by co-treatment with BJP-06–005-3 or BJP-R (Fig. 6c). A 4-day treatment with either dTAG-13 or BJP-06–005-3 alone led to modest viability effects, while their combination had enhanced anti-proliferative activity (Fig. 6d), suggesting that the viability effects of mutant KRAS degradation are amplified by Pin1 inhibition in PATU-8988T cells.

DISCUSSION

Despite decades of research highlighting Pin1 as an oncogenic driver, the development of selective Pin1 inhibitors has proven challenging. Achieving potency generally requires anionic compounds to interact with Pin1's phosphate binding pocket, diminishing cell permeability[22,44]. On the other hand, reported cell-penetrant Pin1 inhibitors are non-selective. Numerous studies feature juglone, which has known off-targets like RNA Polymerase II[45], ATRA[11], which degrades Pin1 but also targets the retinoic acid receptors, and KPT-6566[13], which releases a quinone-mimetic substructure after Pin1 binding that engages a host of other proteins to induce an oxidative stress response. This study describes the first selective, covalent Pin1 inhibitor, BJP-06–005-3, suitable for investigating Pin1 biology. The selectivity of BJP-06–005-3 is currently unparalleled, with Pin1 Cys113 being the only competitively labeled cysteine proteome-wide.

We found Pin1 inhibition to be largely non-toxic after 4-day treatments in 2D-cell culture. This result was validated using the dTAG system, highlighting that BJP-06–005-3's negligible acute cytotoxicity could not be explained by differences in Pin1 inhibition versus degradation. Given the critical role of Pro-directed phosphorylation, this lack of cytotoxicity is surprising and may be explained by upregulation of another PPIase to compensate for Pin1 inhibition, though this remains to be explored.

We also demonstrated that Pin1 cooperates with activated KRAS to drive cell transformation, and that Pin1 loss in the context of 3D-spheroids induced more pronounced anti-proliferative effects than in 2D-monolayers. However, Pin1 inhibition did impact cancer cell viability in 2D-cell culture following prolonged treatments, suggesting that Pin1-mediated growth defects become more pronounced over time. Accordingly, we observed a time-dependent growth dependence on Pin1 using a CRISPR-based GFP dropout assay.

However, this growth effect was modest in comparison to that of an essential protein, 40S Ribosomal Protein S19 (RPS19). We hypothesize that the time-dependent cytotoxicity observed upon Pin1 loss may be explained by minor defects in cell cycle progression, though this requires further study.

Collectively, this study suggests that Pin1 inhibition could prove a viable therapeutic strategy in PDAC and highlights that 3D cell culture models and prolonged treatments best predict Pin1 dependency. Future efforts to cyclize and/or depeptidize BJP-06–005-3 could improve its cell permeability and stability. Also, studies to identify synthetic lethal interactions may reveal suitable drug combinations to enhance therapeutic efficacy. We envision that BJP-06–005-3 and future analogs, as well as the genetic and chemical-genetic tools described herein, will further our understanding of Pin1 biology in disease-relevant contexts.

ONLINE METHODS

Fluorescence Polarization Binding Assay

Binding affinity to Pin1 was determined using a fluorescence polarization (FP) assay to assess competition with an N-terminal fluorescein-labeled peptide (Bth-D-phos.Thr-Pip-Nal), which was synthesized by a peptide synthesis company. The indicated concentrations of candidate compound were pre-incubated for 12 h at 4°C with a solution containing 250 nM glutathione *S*-transferase (GST)-Pin1, 5 nM of fluorescein-labeled peptide probe, 10 μg/ml bovine serum albumin (BSA), 0.01% Tween-20 and 1 mM DTT in a buffer of 10 mM HEPES, 10 mM NaCl and 1% glycerol (pH 7.4). Measurements of FP were made in black 384-well plates (Corning) using an EnVision reader. K_i values obtained from the FP assay results were derived from the Kenakin K_i equation: Kenakin $K_i = (Lb)(EC_{50})(K_d)/(Lo)(Ro) + Lb(Ro–Lo + Lb–K_d)$, where K_d [M]: K_d of the probe, EC_{50} [M]: concentration of unlabeled compound that results in 50% inhibition of binding (obtained from FP assay), total tracer Lo [M]: probe concentration in FP, bound tracer Lb [M]: 85%, fraction of probe bound to Pin1, total receptor Ro [M]: Pin1 concentration in the FP assay, as described[46]. To determine the k_{inact}/K_i, the FP assay was performed following 0, 5, 10, 15, 20, 25, or 30 min incubation times of recombinant Pin1 and BJP-06–005-3 (in a 9-point dose course). The observed rate constant for inhibition, k_{obs}, was determined at each concentration, and was plotted against inhibitor concentration and fitted to a hyperbolic equation (GraphPad software), according to the equation $k_{obs} = k_{inact}[I]/(K_i+[I])$, as described previously[13].

Chemical Synthesis

Synthetic procedures are provided in the Supplementary Note.

PPIase Isomerase Inhibition Assay

Inhibition of Pin1 isomerase activity was determined using the chymotrypsin-coupled PPIase assay, using GST-Pin1 and Suc-Ala-pSer-Pro-Phe-pNA peptide substrate, as described previously[47]. GST-Pin1 was pre-incubated with the indicated concentrations of compound for 12 h at 4°C in buffer containing 35 mM HEPES (pH 7.8), 0.2 mM DTT, and 0.1 mg/mL BSA. Immediately before the assay was started, chymotrypsin (final

concentration of 6 mg/mL), followed by the peptide substrate (Suc-Ala-pSer-Pro-Phe-pNA peptide substrate, final concentration 50 mM) was added. The K_i value obtained from the PPIase assay was derived from the Cheng–Prusoff equation, $K_i = IC_{50}/ (1 + S/K_m)$, where K_m is the Michaelis constant for the peptide substrate, S is the initial concentration of the substrate in the assay, and IC_{50} is the half-minimal inhibitory concentration of the inhibitor.

Covalent Labeling by Intact Mass Spectrometry

5 μg of purified Pin1 protein in 50 μL of 20 mM HEPES pH 7.5 and 75 mM NaCl was incubated with 5 μM of respective Pin1 inhibitors for 0–3 h. A Shimadzu XR HPLC was used to inject the entire sample onto a self-packed reverse-phase column (1/32 in outer diameter × 500 μm inner diameter, 5 cm of POROS 50R2 resin). After desalting, protein was eluted with an HPLC gradient (0%–100% B in 4 min, A = 0.2 M acetic acid in water, B = 0.2 M acetic acid in acetonitrile, flow rate = 10 μl/min) into a LTQ XL mass spectrometer (Thermo Fisher Scientific, San Jose, CA, USA). LTQ XL MS spectra were acquired in centroid mode using the electron multipliers for ion detection. Mass spectra were deconvoluted using MagTran1.03b2 software[48].

Recombinant Protein Labeling Site Identification

Pin1 protein was incubated with indicated compounds for 1 h at room temperature in 20 mM HEPES, 75 mM NaCl, 1 mM TCEP. Protein was reduced with 10 mM TCEP at room temperature (RT) for 30 min, alkylated with 20 mM iodoacetamide (IAA) at RT for 30 min, then digested with trypsin at 37°C overnight. Desalted peptides were analyzed by CE-MS using a ZipChip CE system and autosampler (908 Devices, Boston, MA) interfaced to a Q Exactive HF mass spectrometer (ThermoFisher Scientific, San Jose, CA). Protein solutions were loaded for 30 seconds and separation performed at 500 V/cm for 6 minutes using an HR chip (22 cm separation channel) with a background electrolyte composed of 1% formic acid in 50% acetonitrile. Pressure assist was utilized and started at 1 minute. The mass spectrometer was operated in data-dependent mode and subjected the 5 most abundant ions in each MS scan (15k resolution, 1E6 target, lock mass enabled) to MS/MS (15k resolution, 2E5 target, 100 ms max inject time). Dynamic exclusion was enabled with a repeat count of 1 and an exclusion time of 6 seconds. MS/MS spectra of inhibitor-modified peptides were annotated using mzStudio[49].

Cell Culture

PATU-8988T (DSMZ), PATU-8902 (DSMZ), HeLa (ATCC), MDA-MB-468 (ATCC), 293FT (Thermo Fisher Scientific), Phoenix-AMPHO (ATCC) and HEK293 (ATCC) cells were cultured in Dulbecco’s modified Eagle’s medium (DMEM) supplemented with 10% fetal bovine serum (Sigma) and 1% penicillin/streptomycin. BxPC-3 (ATCC), PC-3 (ATCC), NB4 (ATCC), and Kuramochi (Panagiotis A. Konstantinopoulos’s laboratory) cells were cultured in RPMI supplemented with 10% fetal bovine serum (Sigma) and 1% penicillin/streptomycin. NIH/3T3 (ATCC) cells were cultured in DMEM supplemented with 10% calf serum (Sigma) and 1% penicillin/streptomycin. All cell lines were cultured at 37 °C in a humidified chamber. Cell lines were routinely tested for the absence of Mycoplasma infection.

Establishment of Pin1 KO cell lines using CRISPR/Cas9

Pin1-targeting guides were annealed into the BbsI restriction site of the pX458 plasmid (Addgene cat#48138). The gRNA sequence used was: CAGTGGTGGCAAAAACGGGC. Cells were transfected using the Neon Transfection System (Life Technologies) according to manufacturer guidelines, and GFP+ cells were sorted using fluorescence-activated cell sorting (FACS) using a J AriaII SORP UV machine (BD). Single cell clones were isolated from the bulk-sorted population using limiting dilution plating in a 96-well plate. Once clones were isolated, they were verified for Pin1 knockout by western blotting and by genomic DNA PCR using the following primers: forward: GAGCCTGTGGCACATGGTG, reverse: CAGGGTCAGGTCATGCACTG, sequencing: CTGGCTTCTGGCTGTG, and sequences were analyzed using Tracking of Indels by Decomposition (TIDE)[50].

Generation of stable Dox-inducible and FKBP12^{F36V}-Pin1 cell lines

The Dox-inducible Pin1 construct (pCW57.1-Pin1) was generated by using gateway recombination cloning technology (Invitrogen) to insert the Pin1 coding sequence from a pDONR221-Pin1 donor vector into the pCW57.1 plasmid (Addgene cat#41393) as described previously[20]. The Pin1 sequence in the donor vector was rendered insensitive to the Pin1 gRNA using QuikChange II Mutagenesis (Agilent cat #200521) according to manufacturer's instruction with the following primers: [forward] GTGGCAAAAACGGGCAAGGGGAGCCTGCCAGGGTC and [reverse] GACCCTGGCAGGCTCCCCTTGCCCGTTTTTGCCAC. The N-terminal FKBP12^{F36V}-Pin1 construct (pLEX_305-N-dTAG-Pin1) was generated by using gateway recombination cloning technology (Invitrogen) to insert the Pin1 coding sequence from a pDONR221-Pin1 donor vector into pLEX_305-N-dTAG as described previously[20]. To generate lentivirus, 293FT cells were co-transfected with 2.5μg VSV-G pMD2 (Addgene #12259), 3.75μg psPAX2 (Addgene #12260) and 5μg expression plasmid (either pCW57.1-Pin1 or pLEX_305-N-dTAG-Pin1) using Lipofectamine 2000 according to manufacturer protocol (Thermo Fisher Scientific). Viral particles were collected 48 h after transfection and filtered through a 0.45 μm membrane. Viral supernatants were applied to PATU-8988T Pin1$^{-/-}$ C2 or NIH/3T3 cells in the presence of 8 μg/mL polybrene or NIH/3T3 FKBP12^{F36V}-KRAS^{G12V} cells in the presence of 4 μg/mL polybrene, and transduced cells were selected with 2 μg/mL puromycin.

Generation of stable Pin1 mutant cell lines

Cloning of pBybe Puro Pin1 WT, pBabe Hygro Pin1 W34A and pBabe Hygro Pin1 K63A was described previously[28]. pBybe Pin1 C113S was generated by using QuikChange II (Agilent) according to manufacturer protocol, and sequence was confirmed using the M13-F primer from Genewiz. Lentivirus production and concentration was performed upon transfection of 293FT cells with pBybe Puro Pin1 WT or pBybe Puro Pin1 C113S as previously described[43]. Concentrated viral supernatants were applied to PATU-8988T Pin1$^{-/-}$ C2 cells in the presence of 4 μg/mL polybrene, and transduced cell lines were selected with 2 μg/mL puromycin. Retrovirus production was performed using Phoenix-AMPHO cells, which were transfected with pBabe Hygro Pin1 W34A or pBabe Hygro Pin1 K63A using Fugene 6 (Promega), according to the manufacturer's instructions. Viral

particles were collected 48 h after transfection, filtered through a 0.45 μm membrane, and concentrated using 1:3 Retro-X Concentrator (Clontech), according to the manufacturer's instructions. Concentrated viral supernatants were applied to PATU-8988T Pin1$^{-/-}$ C2 cells in the presence of 4 μg/mL polybrene, and transduced cells were selected with 250 μg/mL hygromycin.

Generation of stable FKBP12^{F36V}-KRAS^{G12V} cell lines

Generation of NIH/3T3 FKBP12^{F36V}-KRAS^{G12V} cells were previously described[20]. Generation of PATU-8988T FKBP12^{F36V}-KRAS^{G12V}; *KRAS*$^{-/-}$ cells were previously described[43].

GFP Dropout Assay

Plasmids were generated using oligos from IDT, annealed according to manufacturers protocol and ligated into the BbsI-digested pLRG plasmid (Addgene #65656). GFP CRISPR dropout assay was conducted as described previously[31] with the following modifications. Lentivirus production and concentration was performed upon transfection of 293FT cells with lentiCas9-blast (Addgene, cat#52962) as previously described[20]. Concentrated viral supernatants were applied to PATU-8988T cells in the presence of 4 μg/mL polybrene, and transduced cell lines were selected with 10 μg/mL blasticidin. PATU-8988T cells constitutively expressing Cas9 were infected with pLRG-sgPin1 (1–8) virus, generated as described above and plated in triplicate in a 96-well plate. 3 days after plating, GFP percentage of all cells were assessed using the following protocol: cells were trypsinized using 30 μl 0.5 % trypsin after media was aspirated from all wells. Trypsin was neutralized with the addition of 105 μl of media. 10 μl of each cell suspension was transferred to a new 96-well plate into 90 μl media to continue the experiment. The remaining cells were diluted 1x with PBS and transferred to a 96-well V-bottom plate (Sigma, cat#CLS3894). The percent of GFP+ cells was then assessed using a Guava EasyCyte 8HT (Millipore). Infection was performed such that the initial percent of GFP+ cells measured on day 3 was roughly 50 %. GFP percentage was assessed every 4–5 days following initial reading. GFP+ cells were quantified using the Guava InCyte software.

Immunoblotting—Whole cell lysates for immunoblotting were prepared by pelleting cells from each cell line at 4°C (300 g) for 5 minutes. The resulting cell pellets were washed 1x with ice-cold PBS and then resuspended in the indicated cell lysis buffer. Lysates were clarified at 14,000 rpm for 15 minutes at 4°C prior to quantification by BCA assay (Pierce, cat #23225). Whole cell lysates were loaded into Bolt 4–12% Bis-Tris Gels (Thermo Fisher, cat #NW04120BOX) and separated by electrophoreses at 95 V for 1.5 h. The gels were transferred to a nitrocellulose membrane using the iBlot Gel Transfer at P3 for 6 minutes (Thermo Fisher, cat #IB23001) and then blocked for 1 h at room temperature in Odyssey blocking buffer (LICOR Biosciences, cat #927–50010). Membranes were probed using antibodies against the relevant proteins at 4°C overnight in 20% Odyssey Blocking Buffer in 1x TBST. Membranes were then washed three times with 1x TBST (at least 5 minutes per wash) followed by incubation with the IRDye goat anti-mouse (LICOR, cat #926–32210) or goat anti-rabbit (LICOR, cat #926–32211) secondary antibody (diluted 1:10,000) in 20% Odyssey Blocking Buffer in 1x TBST for 1 h at room temperature. After three washes with

1x TBST (at least 5 minutes per wash), the immunoblots were visualized using the ODYSSEY Infrared Imaging System (LICOR). Antibodies used against various proteins were as follows: Pin1 (1:1,000, Cell Signaling cat #3722), α-Tubulin (1:1000, Cell Signaling cat #3873), phoshpo-cdc2 (Tyr15) (1:1000, Cell Signaling cat #4539), CDK1 (1:1000, Abcam cat #ab131450), HA-Tag (1:1000, Cell Signaling cat #3724), β-catenin (1:1000, Cell Signaling cat #8480), NFκB p65 (1:1000, Cell Signaling cat #6956), c-Myc (1:1000, Cell Signaling cat #5605), GAPDH (1:1000, Cell Signaling cat #2118), β-Actin (1:1000, Cell Signaling cat #3700), histone H3 (1:1000, Cell Signaling cat #9715).

Lysate Pull-Down with BJP-DTB

Cells were lysed in 50 mM HEPES, pH 7.4, 1 mM EDTA, 10% glycerol, 1 mM TCEP, 150 mM NaCl, 1 mM EDTA, 0.5% NP-40, and protease inhibitor tablet (Roche cat #4693159001) for 20 minutes on ice. After clarifying (14,000 rpm for 15 min), lysates were incubated with the indicated concentration of BJP-DTB for the indicated time points at 4°C, using 500 μg of protein per sample. Lysates were then incubated with streptavidin agarose resin (30 μL of 1:1 beads:lysis buffer slurry) (Thermo scientific, cat #20349) for 1 h at 4°C. Beads were washed four times with 500 μL of washing buffer (50 mM HEPES, pH7.5, 10 mM NaCl, 1 mM EDTA, 10 % glycerol), then pelleted by centrifugation and dried. The beads were boiled for 5 minutes at 95°C in 30 μL of 2x LDS + 5% β-mercaptoethanol. Lysates were probed for specified proteins by western blotting using the Bolt system (Life Technologies).

Cellular Target Engagement – Competition with BJP-DTB

PATU-8988T, PC3, or MDA-MB-468 cells were plated in 10 cm plates with 2.5 million cells per plate in 6 mL of media. The day after plating, cells were treated with the indicated concentrations of candidate inhibitor for the indicated time points. The cells were then washed two times with cold PBS (1 mL per 10 cm plate) and collected by scraping with a cell scraper. Cells were lysed in 50 mM HEPES, pH 7.4, 1 mM EDTA, 10% glycerol, 1 mM TCEP, 150 mM NaCl, 1 mM EDTA, 0.5% NP-40, and protease inhibitor tablet (Roche) – using 210 μL of cell lysis buffer per 10 cm plate of cells. After clarifying (14,000 rpm for 15 min), 5 μL of each lysate sample was combined with 5 μL of 2x LDS + 5% β-mercaptoethanol, boiled for 5 minutes, and set aside for the input loading control (later to be loaded directly in the gel). Then, 200 μL of each lysate sample was incubated with 1 μM of BJP-DTB for 1 h at 4°C and processed as in “lysate pull-down with BJP-DTB” (above).

Pin1 Stability Assays: CHX chase

PATU-8988T cells were plated in 6-well plates at a density of 50,000 cells per well in 2 mL media. The day after plating, cells were treated with either DMSO or BJP-06–005-3 for 24 h. The media was then aspirated and replaced with fresh media containing cycloheximide (100 μg/mL) to block new protein synthesis. Cells were harvested at the indicated time points by washing two times with ice-cold 1x PBS, and then lysing in the plate with 100 μL of RIPA lysis buffer per well (Sigma, cat #R0278) supplemented with protease and phosphatase inhibitor tablets (Roche cat #4906845001). Samples were normalized and prepped in 4x LDS + 10% β-mercaptoethanol and boiled for 5 minutes at 95°C. Lysates

were probed for specified proteins by western blotting using the Bolt system (Life Technologies).

BJP-06–005-3 Stability Studies

PATU-8988T cells were plated at a density of 25,000 cells per well in a 24-well plate, with 1 mL of media per well. The day after plating, cells were treated with BJP-06–005-3 (10 μM). 100 μL of media off of the cells was collected at the indicated time points. In parallel, pure media (DMEM + 10% FBS + 1% penstrep) was incubated with 10 μM of BJP-06–005-3 at room temperature, with 100 μL of media collected at the indicated time points. 1 μL of each media sample was Ziptip (Millipore) C18 desalted, mixed with α-Cyano-4-hydroxycinnamic acid matrix and spotted for MALDI MS analysis. Samples were analyzed on an Ab Sciex 4800 MALDI TOF/TOF. Maximum intensity of the BJP-06–005-3 peak was measured in triplicate and averaged for each sample. Decay curves were generated using Prism. N=3 biological replicates were used for each treatment

Cell Cycle Analysis

PATU-8988T cells (parental or C2 + $FKBP12^{F36V}$-Pin1) were plated at 100,000 cells per well in a 6-well plate, with 2 mL of media per well. The day after plating, cells were treated with the indicated concentrations of BJP-06–005-3 or dTAG-13. At the indicated time points, cells were harvested using trypsin, and then washed 3x with cold PBS. Cell pellets were then fixed with 1 mL cold 80% ethanol in PBS at 4°C overnight. The cell pellets were then washed by adding 1 mL of PBS and then centrifuging (1500 rpm for 5 minutes), followed by aspiration of the PBS/ethanol mix. Cells were resuspended in cell cycle staining solution (100 μg/mL of RNAse A (Roche, 10109169001) and 50 μg/mL propidium iodide (Life Technologies, P1304MP), diluted in PBS) and incubated for 10 minutes at room temperature. Cell cycle data was acquired by flow cytometry on a Guava easyCyte flow cytometer (Millipore) using the InCyte software. Data was analyzed using FlowJo. N=3 biological replicates were used for each treatment condition.

Cell Viability Assays: Growth Over Time in 2D-Adherent Monolayer Cell Culture

Cells were plated at a density of 100 cells per well in 100 μL media in a 96-well white clear bottom plate (Corning cat #3903), with at least one plate per time point (Day 0, 2, 4, 6, etc.). Cells were treated the day after plating with 1 μL of DMSO, BJP-06–005-3, BJP-R, or dTAG-13 to give the indicated concentrations, and were then incubated at 37°C 5% CO_2. Every 48 h, the media was aspirated and replaced with fresh media containing fresh compound or DMSO. For the Dox-inducible PATU-8988T $Pin1^{-/-}$ C2 cells, the media was replenished with Dox (100 ng/mL), in addition to compound or DMSO, every 48 h. For PATU-8988T $Pin1^{-/-}$ C2 cells expressing Pin1 WT, C113S, W34A or K63A, the media was replenished after 96 h. When the indicated time points had been reached, cell viability was evaluated using the CellTiter-Glo Luminescent Cell Viability Assay (Promega cat#G7570) according to the manufacturer's standards, measuring luminescence using an Envision plate-reader. To normalize for differences in plating density between cell lines, a duplicate Day 0 plate of cells was plated at the beginning of the experiment and exposed using CellTiter-Glo (Promega cat #G7570) the day after plating, prior to compound treatment. At least n = 3 biological replicates were used for each treatment condition.

Cell Viability Assays: 4-Day Treatment in 2D-Adherent Monolayer Cell Culture

PATU-8988T cells were plated in flat bottom 96-well plates (Corning cat #3903) at a density of 1,000 cells per well in 100 uL media and were treated the next day with 1 μL of the indicated compounds in a three-fold dilution series. The cells were incubated at 37°C 5% CO_2 and, when indicated, every 24 h the media was aspirated and replaced with fresh media/retreated with fresh compound to ensure maximal Pin1 engagement for the duration of the experiment. 96 h after the initial treatment, anti-proliferative effects were assessed by CellTiter-Glo Luminescent Cell Viability Assay (Promega cat #G7570) according to the manufacturer's standards, measuring luminescence using an Envision plate-reader. N=3 biological replicates were used for each treatment condition.

Inhibitor Effects on Pin1 Downstream Signaling and Pin1 Degradation

Cells were plated in 6-well plates at a density of 100,000 cells per well in 2 mL media. The day after plating, cells were treated with DMSO or the indicated concentrations of BJP-06–005-3, BJP-R, dTAG-13, or Dox. For the Wnt3a experiment (Supplementary Figure 10f), cells were treated for 4 h with DMSO, BJP-06–005-3, or BJP-R, followed by treatment with either DMSO or recombinant human Wnt3a (50 ng/mL) (R&D systems, cat #5036) for an additional 4 h. Cells were harvested at the indicated time points by washing two times with ice-cold 1x PBS, and then lysing in the plate with 100 μL of RIPA lysis buffer per well (Sigma, cat #R0278) supplemented with protease and phosphatase inhibitor tablets (Roche cat #4906845001). Samples were normalized and prepped in 4x LDS + 10% β-mercaptoethanol and boiled for 5 minutes at 95°C. Lysates were probed for specified proteins by western blotting using the Bolt system (Life Technologies).

Ultra-Low Adherent (ULA) 3D-Spheroid Assay

Cells were plated in clear, round bottom ULA 96-well plates (Corning cat #07201680) at a density of 1,000 cells per well in 100 μL media. After plating, cells were spun at 300 g for 5 minutes. The day after plating, cells were treated with DMSO or the indicated concentrations of BJP-06–005-3. 48 h after the initial treatment, cells were re-treated with DMSO or BJP-06–005-3. 96 h after the initial treatment, cell viability was evaluated using CellTiter-Glo (Promega cat #G7570). To normalize for differences in plating density between cell lines, a duplicate Day 0 plate of cells was plated at the beginning of the experiment and exposed using CellTiter-Glo (Promega cat #G7570) the day after plating. The final absorbance was then divided by the average Day 0 reading to normalize according to initial plating density. For direct comparisons to growth in 2D-adherent monolayer cell culture, plating conditions and treatments were performed identically as described for the 3D-Spheroid assay, except that cells were plated in flat bottom 96-well plates (Corning cat #3903). N=3 biological replicates were used for each treatment condition.

Nuclear/Cytoplasmic Fractionation

PATU-8988T cells were plated at a density of 2 million cells per 10 cm plate in 6 mL of media. The next day, cells were treated with either DMSO, BJP-06–005-3, or BJP-R at the indicated concentrations for 5.5 h. Cells were harvested with 0.25% trypsin-EDTA (Thermo Fisher Scientific) (2 mL per 10 cm plate), washed 1x with 1 mL PBS, and then processed

according to the manufacturer protocol using the Thermo Scientific NE-PER Nuclear and Cytoplasmic Extraction Kit (cat #78833). For the Wnt3a treatment and fractionation experiment (Supplementary Figure 10h), cells were treated for 4 h with DMSO, BJP-06–005-3, or BJP-R at the indicated concentrations, followed by treatment with either DMSO or recombinant human Wnt3a (50 ng/mL) (R&D systems, cat #5036) for an additional 4 h., and then cells were harvested and processed as above.

RNA-Sequencing

PATU-8988T cells were plated at a density of 100,000 cells per well in 2 mL of media per well of a 6-well plate. The next day, cells were treated for 4 h with DMSO, 10 μM BJP-06–005-3 or 10 μM BJP-R. To harvest, cells were washed 2x with 1 mL PBS per well and lysed in Buffer RLT Plus (QIAGEN). RNA was extracted using the QIAGEN RNeasy Plus Mini Kit (cat #74134) according to the manufacturer protocol. Samples were sequenced by Invitrogen using the Ion AmpliSeq platform. Analysis of the mapped reads was performed in R using the limma framework[51].

Protein expression and purification

A construct of full-length human Pin1 in a pET28 vector was overexpressed in E. coli BL21 (DE3) in LB medium in the presence of 50 mg/ml of kanamycin. Cells were grown at 37°C to an OD of 0.8, cooled to 17°C, induced with 500 μM isopropyl-1-thio-D-galactopyranoside, incubated overnight at 17°C, collected by centrifugation, and stored at −80°C. Cell pellets were sonicated in buffer A (50 mM HEPES pH 7.5, 300 mM NaCl, 10% glycerol, 10 mM Imidazole, and 3 mM BME) and the resulting lysate was centrifuged at 30,000 ×g for 40 min. Ni-NTA beads (Qiagen) were mixed with lysate supernatant for 30 min and washed with buffer A. Beads were transferred to an FPLC-compatible column and the bound protein was washed with 15% buffer B (50 mM HEPES pH 7.5, 300 mM NaCl, 10% glycerol, 300 mM Imidazole, and 3 mM BME) and eluted with 100% buffer B. Thrombin was added to the eluted protein and incubated at 4°C overnight. The sample was concentrated and passed through a Superdex 200 10/300 column (GE helathcare) in a buffer containing 20 mM HEPES, pH 7.5, 150 mM NaCl, 5% glycerol, 3 mM DTT, and 1 mM TCEP. Fractions were pooled, concentrated to approximately 37 mg/ml and frozen at −80°C.

Crystallization: BJP-02–118-2—Apo protein at a final concentration of 1 mM was crystallized by sitting-drop (200 nL + 200 nL) vapor diffusion at 20°C in the following crystallization buffer: 3 M NH_4SO_4, 100 mM BisTris-pH7.0, 1% PEG400, and 1 mM DTT. A volume of 200 nL of 1 mM BJP-02–118-2 was added directly to crystals for soaking at 20°C for 16 h. Crystals were transferred briefly into crystallization buffer containing 25% glycerol prior to flash-freezing in liquid nitrogen.

Crystallization: BJP-07–017-3—Apo protein at a final concentration of 1 mM was crystallized by sitting-drop (200 nL + 200 nL) vapor diffusion at 20°C in the following crystallization buffer: 3 M NH_4SO_4, 100 mM BisTris-pH7.0, 1% PEG400, and 1 mM DTT. A volume of 1 μL of 100 mM BJP-07–017-3 was mixed with 25 μL mother liquor, and 2 μL of that solution was added to crystal drops. Crystallization wells were resealed, plates were incubated at 20°C for 2 h, and crystals were cryoprotected/harvested as usual.

Crystallization: Data collection and structure determination—Diffraction data from complex crystals were collected at beamline 24ID-C/E of the NE-CAT at the Advanced Photon Source at the Argonne National Laboratory. Data sets were integrated and scaled using XDS[52]. Structures were solved by molecular replacement using the program Phaser[53] and the search model PDB entry 1PIN. Iterative manual model building and refinement using Phenix[54] and Coot[55] led to models with excellent statistics.

CITe-Id Selectivity Assessment

HEK 293 cell pellets were lysed with lysis buffer (50 mM Tris pH 7.5, 150 mM NaCl, 1 mM EDTA, 10% v/v glycerol, 0.5% v/v NP-40, protease inhibitors). After lysate clearance centrifugation, protein concentration was determined by BCA. Samples were precleared with streptavidin resin for 1 h at 4°C. After centrifugation, the supernatant was split in four and pretreated with DMSO or increasing concentrations of BJP-06–005-3 (100 nM, 500 nM, 1 μM) and incubated at room-temperature for 3 h. 2 μM of the desthiobiotin-tagged analog (BJP-DTB) was added to all samples and incubated at 4°C for 18 h. Urea was added to 8 M final concentration followed by cleanup using Zeba™ desalting columns. Samples were diluted to 4 M urea with pH 8 lysis buffer and reduced with 10 mM DTT for 30 min at 56°C. Samples were then alkylated with 20 mM iodoacetamide (IAA) for 30 min at RT. Samples were further diluted to 2 M urea before trypsin digestion at 37°C overnight. Streptavidin resin was added to the samples and incubated at RT for 1 h. The beads were sequentially washed with lysis buffer three times, PBS three times, and water two times. Peptides were eluted with four sequential incubations of 50% acetonitrile (MeCN), 0.1% trifluoroacetic acid (TFA) for 3 min at room temperature. Eluted peptides were concentrated by vacuum centrifugation and resuspended in 0.1% TFA before batch mode C18 cleanup, as described previously56. Samples were vacuum dried and resuspended in 30% 0.5M TEAB, 70% EtOH. iTRAQ stable isotope labeling reagent was added to each corresponding sample. After incubation at RT for 1 h, the samples were combined and acidified before vacuum drying. Samples were reconstituted in 0.1% TFA and desalted using a SOLA desalting plate before vacuum drying. Samples were reconstituted in 25% MeCN, 0.1% TFA and batch mode SCX cleaned, as described previously[56]. Samples were vacuum dried and reconstituted in 5% DMSO, 100 mM ammonium formate for 3D RP-SAX-RP LC-MS/MS[57]. Peptides were separated across eleven fractions using a 90 min 5%−60% MeCN gradient on a Q-Exactive HF mass spectrometer. For data processing, native .RAW data files from the mass spectrometer were processed using the multiplierz Python-based framework[58] to generate .mgf files for input to Mascot (Matrix Science). MS/MS spectra were processed to account for inhibitor fragmentation, as described previously[59]. Peptide precursor masses were recalibrated on a per-scan basis by correcting all m/z values based on accurate mass recorded for the $Si(CH_3)_2O_6$ peak in each spectrum. All data was searched against a forward-reverse human database assembled from the NCBI Refseq database. For de-isotoped HCD spectra, the precursor mass tolerance was set to 10 ppm and the MS/MS fragment ion tolerance was set to 25 mmu. Search parameters included trypsin specificity, with a maximum of two missed cleavages, fixed carbamidomethylation of Cys (+57 Da), variable oxidation on Met (+16 Da with −64 Da neutral loss possible), variable deamidation on Asn and Gln (+1 Da), fixed iTRAQ 4-plex labeling on Lys and N-termini (+144 Da), variable BJP-DTB labeling of Cys (+997 Da, with −997 Da neutral loss possible). Reported

peptide sequences were filtered based on a 1% false discovery rate. Normalized reporter ion signal for labeled cysteine residues from multiple PSMs was summed and a ratio was generated for each reporter channel by comparing it to the DMSO-treated control channel. Inhibitor concentrations and ratios were used to generate a trendline for each labeled site with the slope being the competitive dose response for the cysteine site.

Yeast experiments

To test complementation of yeast Ess1, strain YSB1026 (derived from strain YXW-3, generously provided by Steve Hanes)[60] was transformed with HIS3-marked plasmids expressing yeast Ess1, human Pin1, the FKBP12^{F36V}-Pin1 fusion, or the non-expressing HIS3 vector. Transformants were grown at 30°C overnight in synthetic complete media lacking histidine. After normalizing cell density to ensure that equal numbers of cells were spotted, four-fold serial dilutions were spotted onto the appropriate selective plates. Plates containing 5-fluoro-orotic acid (5FOA) were used to select against pRS426-Pin1, carrying the wild-type Pin1 on a URA3 plasmid. Plates were incubated for three days at 30°C. Although only one set is shown, four biological replicates gave the identical results. To ensure that the FKBP12^{F36V}-Pin1 fusion protein was expressed and intact, whole cell extracts were made by glass bead lysis. 50 micrograms of protein from each strain was separate by standard SDS-PAGE, blotted to nitrocellulose membrane, and probed with antibodies against Pin1. Yeast strains:

YSB1026: MATa, ura3–1, leu2–3,112, trp1–1, his3–11,15, ade2–1, can1–100, ess1Δ:TRP1 (pRS426-Pin1)

Plasmids:

pTPI-Pin1 (Steve Hanes)

pTPI-FKBP^{F36V}-Pin1 (this report)

pRS413-Ess1 (Steve Hanes)

pRS426-Ess1 (this report)

STATISTICS AND REPRODUCIBILITY

Information regarding error bars, number of replicates or samples, and statistical analyses are described in the corresponding figure legends. Experiments were not blinded nor randomized, and sample sizes were not predetermined using statistical analysis.

DATA AVAILABILITY STATEMENT

CITe-Id data for BJP-06–005-3 is provided as an excel file, Supplementary Dataset 1. RNA-sequencing data has been deposited to the NCBI GEO (accession GSE147340), and the analyzed data file is provided as an excel file, Supplementary Dataset 2. All structural data has been deposited in the PDB (PDB codes 6O33, 6O34).

Supplementary Material

Refer to Web version on PubMed Central for supplementary material.

ACKNOWLEDGEMENTS

We thank all members of the Gray lab for helpful discussions, M. Kostic for providing feedback on the manuscript, and K. Westover for discussion of k_{inact} and K_i calculations. This work was supported by the Ruth L. Kirschstein NRSA Individual Predoctoral Fellowship (F31 CA225066, B.J.P), the Training Grant in Pharmacological Sciences (NIH T32 GM007306, B.J.P./Z.M.D.), the Training Grant in Chemical Biology (NIH 5 T32 GM095450-04, B.J.P.), the Chleck Foundation (B.J.P./Z.M.D.), the American Cancer Society Postdoctoral Fellowship (PF-17-010-01-CDD, B.N.), Claudia Adams Barr Program in Innovative Basic Cancer Research Award (B.N.), Katherine L. and Steven C. Pinard Research Fund (N.S.G./B.N.), the Israel Science Foundation (2462/19, N.L.), the Rising Tide Foundation (N.L.), the Israel Cancer Research Fund (N.L.), the Israeli Ministry of Science and Technology (3-14763, N.L.), the Moross integrated cancer center (N.L.), the Helen and Martin Kimmel Center for Molecular Design (N.L.), the Joel and Mady Dukler Fund for Cancer Research (N.L.), the Estate of Emile Mimran, Virgin JustGiving, and the George Schwartzman Fund (N.L.), the National Institutes of Health R01's (R01 GM056663, S.B.), (R01 CA219850, R01 CA233800 J.A.M), (R01 CA205153, N.S.G, K.P.L, and X.Z.Z), and the Hale Center for Pancreatic Research (N.S.G.). BJP-02-118-2 and BJP-07-017-3 co-crystal structures were determined thanks to research conducted at the Advanced Photon Source on the Northeastern Collaborative Access Team beamlines (NIGMS P41 GM103403).

COMPETING FINANCIAL INTERESTS

N.S.G. is a Scientific Founder and member of the Scientific Advisory Board (SAB) of C4 Therapeutics, Syros, Soltego, Gatekeeper and Petra Pharmaceuticals and has received research funding from Novartis, Astellas, Taiho and Deerfield. J.A.M. serves on the SAB of 908 Devices, Boston, MA, and receives sponsored research support from Vertex and AstraZeneca. N.L. is a member of the SAB of Trilogy Sciences and has received research support from Teva. B.J.P, N.S.G, H.-S.S., S.D.-P., Z.M.D., C.M.B., J.A.M, S. Kozono, X.L., K.P.L, and X.Z.Z. are inventors on a patent application related to the Pin1 inhibitors described in this manuscript (WO/2019/241496). B.N. is an inventor on patent applications related to the dTAG system described in this manuscript (WO/2017/024318, WO/2017/024319, WO/2018/148443, WO/2018/148440). K.P.L. and X.Z.Z. are inventors on many issued patents or pending patent applications related to Pin1 inhibitors and/or biomarkers.

REFERENCES

1. Lu Z & Hunter T Prolyl isomerase pin1 in cancer. Cell Research 24, 1033–1049 (2014). [PubMed: 25124924]
2. Lu KP, Finn G, Lee T, & Nicholson LK Prolyl cis-trans isomerization as a molecular timer. Nature Chemical Biology 3, 619–629 (2007). [PubMed: 17876319]
3. Yeh ES & Means AR Pin1, the cell cycle and cancer. Nature Reviews 7, 381–388 (2007).
4. Lu KP, & Zhou XZ The isomerase PIN1 controls numerous cancer-driving pathways and is a unique drug target. Nature Reviews Cancer 16, 463–478 (2016). [PubMed: 27256007]
5. Liang C et al. PIN1 maintains redox balance via the c-Myc/NRF2 axis to counteract Kras-induced mitochondrial respiratory injury in pancreatic cancer cells. Cancer Res. Doi: 10.1158/0008-5472.CAN-18-1968 (2019).
6. Wulf G, Garg P, Liou YC, Iglehart D, & Lu KP Modeling breast cancer *in vivo* and *ex vivo* reveals an essential role of Pin1 in tumorigenesis. EMBO J. 23, 3397–3407 (2004). [PubMed: 15257284]
7. Zeitouni D, Pylayeva-Gupta Y, Der CJ, & Bryant KL KRAS Mutant Pancreatic Cancer: No Lone Path to an Effective Treatment. Cancers (Basel) 8, 45 (2016).
8. Hanes SD The Ess1 prolyl isomerase: traffic cop of the RNA polymerase II transcription cycle. Biochim. Biophys. Acta. 4, 316–333 (2014).
9. Liou YC et al. Loss of Pin1 function in the mouse causes phenotypes resembling cyclin D1-null phenotypes. PNAS 99, 1335–1430 (2001).
10. Hennig L et al. Selective inactivation of parvulin-like peptidyl-prolyl *cis*/*trans* isomerases by juglone. Biochemistry 37, 5953–5960 (1998). [PubMed: 9558330]
11. Wei S et al. Active Pin1 is a key target of all-*trans* retinoic acid in acute promyelocytic leukemia and breast cancer. Nature Med. 21, 457–466 (2015). [PubMed: 25849135]

12. Kozono S et al. Arsenic targets Pin1 and cooperates with retinoic acid to inhibit cancer-driving pathways and tumor-initiating cells. Nature Communications 9, (2018).
13. Campaner E et al. A covalent PIN1 inhibitor selectively targets cancer cells by a dual mechanism of action. Nature Communications 8, 15772 (2017).
14. Ieda N et al. An irreversible inhibitor of peptidyl-prolyl cis/trans isomerase Pin1 and evaluation of cytotoxicity. Bioorganic & Medicinal Chemistry Letters 29, 353–356 (2018). [PubMed: 30585173]
15. Moore JD & Potter A Pin1 inhibitors: Pitfalls, progress and cellular pharmacology. Bioorg. Med. Chem. Lett 23, 4283–4291 (2013). [PubMed: 23796453]
16. Mah R, Thomas JR, & Shafer CM Drug discovery considerations in the development of covalent inhibitors. Bioorganic & Med. Chem. Letters 24, 33–39 (2014).
17. Liu Q, Sabnis Y, Zhao Z, Zhang T, Buhrlage SJ, Jones LH, & Gray NS Developing irreversible inhibitors of the protein kinase cysteinome. Chem Biol 20, 146–159 (2013). [PubMed: 23438744]
18. Chen CH et al. Pin1 cysteine-113 oxidation inhibits its catalytic activity and cellular function in Alzheimer's disease. Neurobiol. Dis 76, 13–23 (2015). [PubMed: 25576397]
19. Zhang Y et al. Structural basis for high-affinity peptide inhibition of human Pin1. ACS Chem Biol 2, 320–328 (2007). [PubMed: 17518432]
20. Nabet B et al. The dTAG system for immediate and target-specific protein degradation. Nature Chemical Biology 14, 431–441 (2018). [PubMed: 29581585]
21. Backus KM et al. Proteome-wide covalent ligand discovery in native biological systems. Nature 534, 570–574 (2016). [PubMed: 27309814]
22. Guo C et al. Structure-based design of novel human Pin1 inhibitors (III): Optimizing affinity beyond the phosphate recognition pocket. Bioorganic & Med. Chem. Letters 24, 4187–4191 (2014).
23. Yang NJ, & Hinner MJ Getting across the cell membrane: an overview for small molecules, peptides, and proteins. Methods Mol Biol 1266, 29–53 (2015). [PubMed: 25560066]
24. Singh J, Petter RC, Baillie TA & Whitty A The resurgence of covalent drugs. Nat. Rev. Drug Discov 10, 307–317 (2011). [PubMed: 21455239]
25. Valley CC et al. The methionine-aromatic motif plays a unique role in stabilizing protein structure. JBC 287, 34979–34991 (2012).
26. Browne CM et al. A chemoproteomic strategy for direct and proteome-wide covalent inhibitor target-site identification. J. Am. Chem. Soc 141, 191–203 (2019). [PubMed: 30518210]
27. Long MJ, Gollapalli DR, & Hedstrom L Inhibitor mediated protein degradation. Chem Biol 19, 629–637 (2012). [PubMed: 22633414]
28. Luo ML et al. Prolyl isomerase Pin1 acts downstream of miR-200 to promote cancer stem-like cell traits in breast cancer. Cancer Res. 74, 3603–3616 (2014). [PubMed: 24786790]
29. Rotem A et al. Alternative to the soft-agar assay that permits high-throughput drug and genetic screens for cellular transformation. PNAS 112, 5708–5713 (2015). [PubMed: 25902495]
30. Janes MR et al. Targeting KRAS Mutant Cancers with a Covalent G12C-Specific Inhibitor. Cell 172, 578–589 (2018). [PubMed: 29373830]
31. Shi J, Wang E, Milazzo JP, Wang Z, Kinney JB, & Vakoc CR Discovery of cancer drug targets by CRISPR-Cas9 screening of protein domains. Nat. Biotechnol 33, 661–667 (2015). [PubMed: 25961408]
32. Erb MA et al. Transcription control by the ENL YEATS domain in acute leukemia. Nature 543, 270–274 (2017). [PubMed: 28241139]
33. Behrsin CD et al. Functionally important Residues in the Peptidyl-prolyl Isomerase Pin1 Revealed by Unigenic Evolution. J. Mol. Biol 365, 1143–1162 (2007). [PubMed: 17113106]
34. An S, & Liwu F Small-molecule PROTACs: an emerging and promising approach for the development of targeted therapy drugs. EBioMedicine 36, 553–562 (2018). [PubMed: 30224312]
35. Tzur A, Kafri R, LeBleu VS, Lahav G, & Kirschner MW Cell growth and size homeostasis in proliferating animal cells. Science 325, 167–171 (2009). [PubMed: 19589995]
36. Crenshaw DG, Yang J, Means AR, & Kornbluth S The mitotic peptidyl-prolyl isomerase, Pin1, interacts with Cdc25 and Plx1. The EMBO Journal 17, 1315–1327 (1998). [PubMed: 9482729]

37. Ryo A, Nakamura M, Wulf G, Liou YC, & Lu KP Pin1 regulates turnover and subcellular localization of beta-catenin by inhibiting its interaction with APC. Nat. Cell Biol 9, 793–801 (2001).
38. Ryo A et al. Regulation of NF-kappaB signaling by Pin1-dependent prolyl isomerization and ubiquitin-mediated proteolysis of p65/RelA. Mol. Cell 12, 1413–1426 (2003). [PubMed: 14690596]
39. Yeh E et al. A signaling pathway controlling c-Myc degradation that impacts oncogenic transformation of human cells. Nat. Cell Biol 6, 308–318 (2004). [PubMed: 15048125]
40. Kuleshov MV et al. Enrichr: a comprehensive gene set enrichment analysis web server 2016 update. Nucleic Acids Res. 44 (Web Server issue), W90–W97. 10.1093/nar/gkw377. [PubMed: 27141961]
41. Farrell AS et al. Pin1 regulates the dynamics of c-Myc DNA binding to facilitate target gene regulation and oncogenesis. Molecular and Cellular Biology 33, 2930–2949 (2013). [PubMed: 23716601]
42. Vaseva AV et al. KRAS Suppression-Induced Degradation of MYC Is Antagonized by a MEK5-ERK5 Compensatory Mechanism. Cancer Cell 34, 807–822 (2018). [PubMed: 30423298]
43. Ferguson FM et al. Discovery of a selective inhibitor of Doublecortin Like Kinase 1. Nature Chemical Biology In Press (2020).
44. Spena CR et al. Liposomal delivery of a Pin1 inhibitor complexed with cyclodextrins as new therapy for high-grade serious ovarian cancer. J. of Controlled Release 281, 1–10 (2018).
45. Chao SH, Greenleaf AL, & Price DH Juglone, an inhibitor of the peptidyl-prolyl isomerase Pin1, also directly blocks transcription. Nucleic Acids Res. 29, 767–773 (2001). [PubMed: 11160900]

METHODS ONLY REFERENCES

46. Auld DS et al. Receptor binding assays for HTS and drug discovery in Assay Guidance Manual eds. Sittampalam GS, et al. Eli Lilly & Company and the National Center for Advancing Translational Sciences (2004).
47. Yaffe MB et al. Sequence-specific and phosphorylation-dependent proline isomerization: A potential mitotic regulatory mechanism. Science 278, 1957–1960 (1997). [PubMed: 9395400]
48. Zhang Z & Marshall AG A universal algorithm for fast and automated charge state deconvolution of electrospray mass-to-charge ratio spectra. J Am Soc Mass Spectrom 9, 225–233, doi:10.1016/S1044-0305(97)00284-5 (1998). [PubMed: 9879360]
49. Ficarro SB, Alexander WM, & Marto JA mzStudio: a dynamic digital canvas for user-driven interrogation of mass spectrometry data. Proteomes 5, 20 (2017).
50. Brinkman EK, Chen T, Amendola M, & Steensel BV Easy quantitative assessment of genome editing by sequence trace decomposition. Nucleic Acids Research 42(22), e168 (2014). [PubMed: 25300484]
51. Ritchie ME et al. Limma powers differential expression analyses for RNA-sequencing and microarray studies. Nucleic Acids Research 43(7), e47 (2015). [PubMed: 25605792]
52. Kabsch W Integration, scaling, space-group assignment and post-refinement. Acta Cryst. 66, 133–144 (2010).
53. McCoy AJ, Gross-Kunstleve RW, Adams PD, Winn MD, Storoni LC, Read RJ Phaser crystallographic software. J. Appl. Cryst. 40, 658–674 (2007). [PubMed: 19461840]
54. Adams PD et al. PHENIX: a comprehensive Python-based system for macromolecular structure solution. Acta Cryst. 66, 213–221 (2010).
55. Emsley P, & Cowtan K Coot: model-building tools for molecular graphics. Acta Cryst. 60, 2126–2132 (2004).
56. Adelmant GO, C. J., Ficarro SB, Sikorski TW, Zhang Y, Marto JA. in Sample Preparation in Biological Mass Spectrometry (ed · Lazarev AV Ivanov AR) Ch. 22, (Springer)
57. Zhou F et al. Genome-scale proteome quantification by DEEP SEQ mass spectrometr y. Nat Commun 4, 2171, doi:10.1038/ncomms3171 (2013). [PubMed: 23863870]

58. Parikh JR et al. Multiplierz: an extensible API based desktop environment for proteomics data analysis. BMC bioinformatics 10, 364, doi:10.1186/1471-2105-10-364 (2009). [PubMed: 19874609]

59. Ficarro SB et al. Leveraging gas-phase fragmentation pathways for improved identification and selective detection of targets modified by covalent probes. Anal Chem. 88, 12248–12254 (2016). [PubMed: 28193034]

60. Wu X et al. The Ess1 prolyl isomerase is linked to chromatin remodeling complexes and the general transcription machinery. EMBO J. 19, 3727–3738 (2000). [PubMed: 10899126]

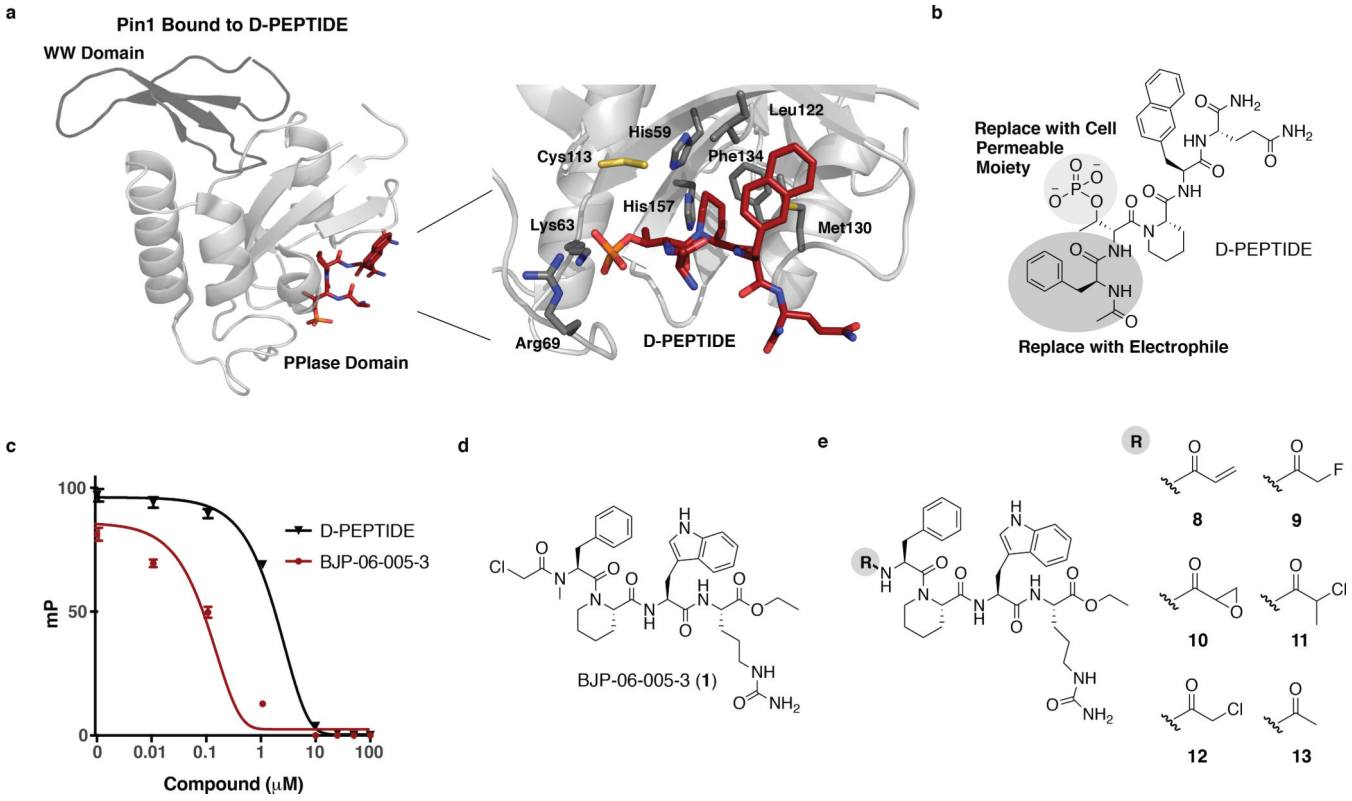

Figure 1 |. Structure-guided modification of D-PEPTIDE to yield optimized Pin1 binders.

(**a**) Structure of D-PEPTIDE (red) bound to Pin1, with the PPIase domain in light gray, and the WW domain in dark gray (left). Zoomed structure of D-PEPTIDE (red) in the PPIase active site, with key residues for binding highlighted in dark gray, and Cys113 in yellow (right). PDB 2ITK; (**b**) Plan for structure-guided optimization of D-PEPTIDE to achieve cell permeability and covalency; (**c**) FP readout following a 12 h incubation with Pin1. Data points are plotted as the average of n = 3 independent samples ± SEM, and are representative of n = 3 independent experiments; (**d**) Chemical structure of BJP-06–005-3; (**e**) Chemical structures of derivatives featuring alternate electrophiles.

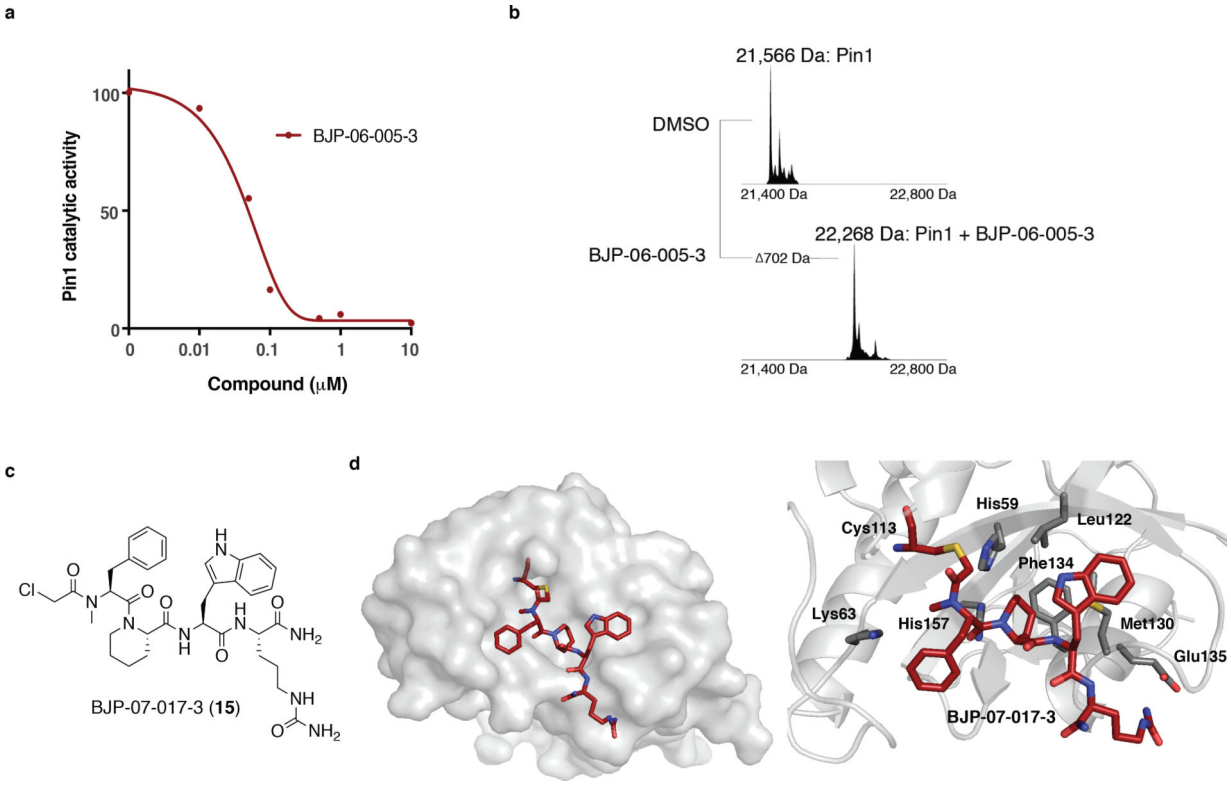

Figure 2 |. Biochemical and structural characterization of BJP-06–005-3.

(**a**) PPIase assay results for BJP-06–005-3 (IC_{50} = 48 nM) after a 12 h incubation with Pin1. Data points are plotted as the mean of n = 2 independent experiments, with each experiment having n = 1 independent samples; (**b**) Intact mass spectrometry of Pin1 after incubation with DMSO or BJP-06–005-3 for 1 h at RT; (**c**) Chemical structure of BJP-07–017-3; (**d**) 1.6 Å co-crystal structure of BJP-07–017-3 (red) covalently bound to Pin1 (light gray) via Cys113, with key binding residues highlighted in dark gray (PDB 6O34).

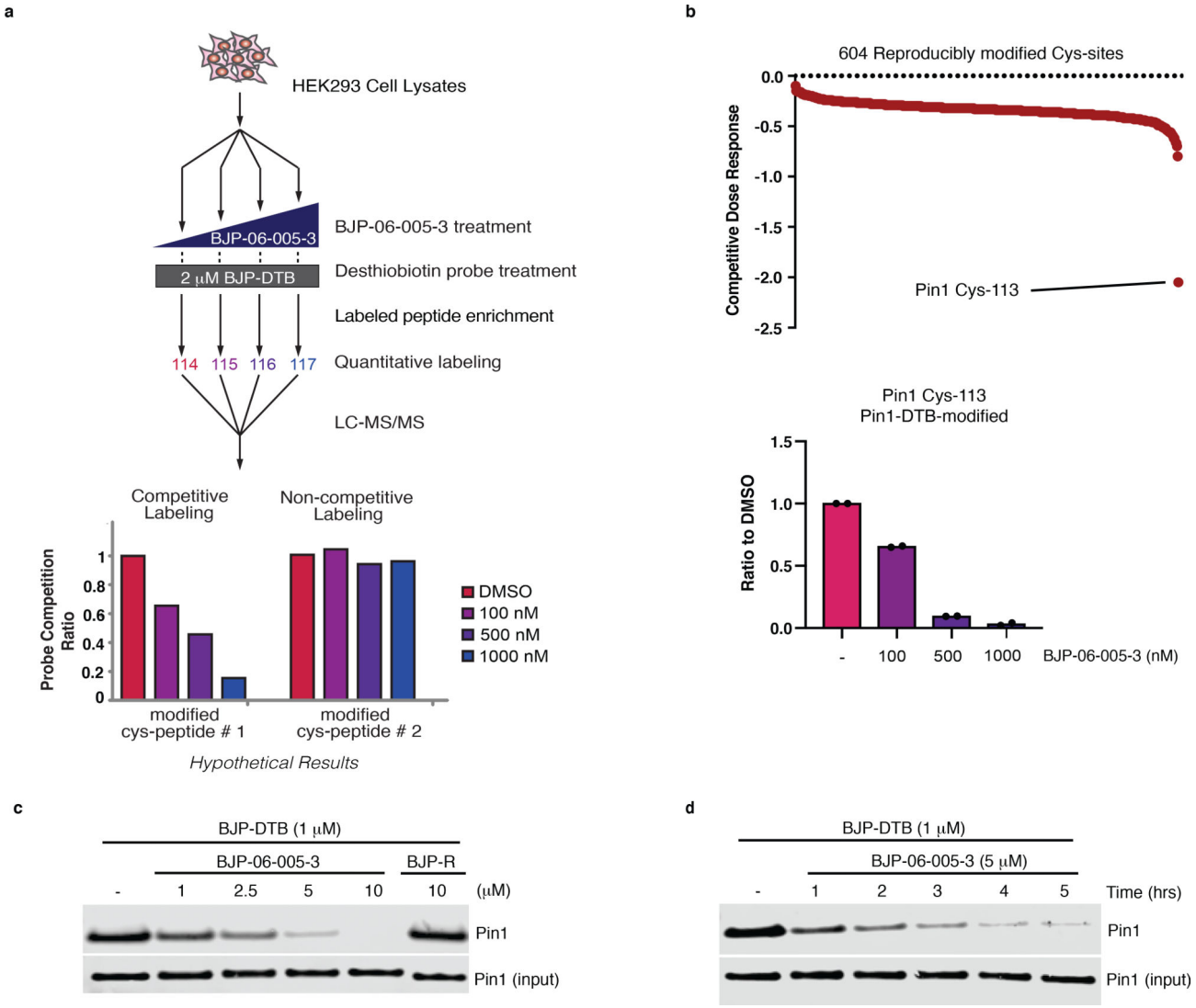

Figure 3 |. BJP-06–005-3 is selective and engages cellular Pin1.

(**a**) Schematic depiction of CITe-Id workflow, showing hypothetical results. CITe-Id directly identifies BJP-DTB modification sites across the proteome and quantifies their affinity for BJP-06–005-3[26]; (**b**) Waterfall plot of the competitive dose responses for the 604 cysteine sites reproducibly modified by BJP-DTB in n = 2 independent experiments. Pin1 Cys113 competitive dose response is 11 standard deviations from the next strongest competing site, and it is the only site with >50% competition at the two highest concentrations (90% competition at 500 nM BJP-06–005-3, 97% competition at 1 μM BJP-06–005-3). The mean peak height of n = 2 biologically independent samples are shown as dot-plots; (**c**) PATU-8988T cells treated in a competition format with the indicated concentrations of BJP-06–005-3 or BJP-R for 5 h, followed by cell lysis, incubation with BJP-DTB, streptavidin pull-down, and immunoblot analysis; (**d**) PATU-8988T cells treated with 5 μM BJP-06–005-3 for the indicated times, followed by cell lysis, incubation with BJP-DTB, streptavidin pull-down, and immunoblot analysis. Uncropped immunoblots for **c**-**d** are

displayed in Supplementary Figure 12, and are representative of n = 4 independent experiments.

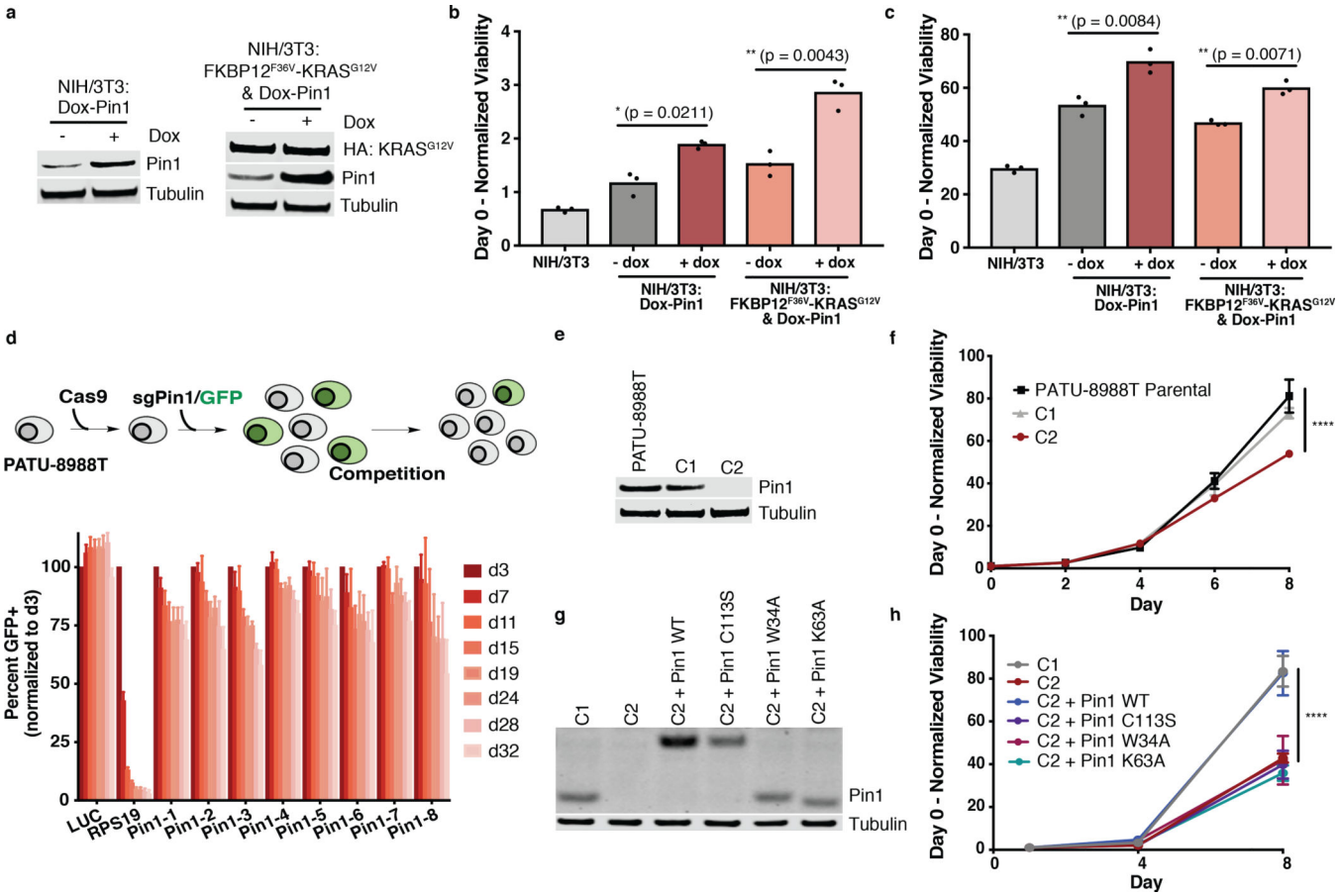

Figure 4 |. Pin1 cooperates with KRAS^{G12V} to promote cell transformation, and Pin1 loss leads to viability defects.

(**a**) Immunoblot analysis of NIH/3T3 cells transduced with Dox-inducible Pin1 alone, or in combination with FKBP12^{F36V}-KRAS^{G12V} (HA-tagged), after Dox treatment (100 ng/mL) for 48 h; (**b**) Day 0-normalized proliferation of the cell lines from **a**, cultured as 3D-spheroid suspensions or as (**c**) 2D-monolayers, with or without Dox (100 ng/mL) for 120 h. The mean peak height of n = 3 biologically independent samples are shown as dot-plots, and are representative of n = 2 independent experiments. P values were determined by Welch's two-sided t-test; (**d**) Schematic of the CRISPR/Cas9 GFP dropout assay (above), GFP+ (sgRNA +) population percentage is depicted at the indicated days following lentiviral transduction in Cas9-expressing PATU-8988T cells (below). Statistics are reported in Supplementary Table 4; (**e**) Immunoblot analysis of lysates from parental PATU-8988T, C1, and C2; (**f**) Day 0-normalized growth rate of C1, C2, and parental PATU-8988T, with readings taken every 2 days. **** adj. $p < 0.0001$ by Bonferroni-corrected two-way ANOVA; (**g**) Immunoblot analysis of lysates from C1, C2, and C2 transduced with Flag-Pin1 (WT or C113S) or Pin1 (W34A or K63A); (**h**) Day 0-normalized growth rate of C1, C2, or C2 transduced with Flag-Pin1 (WT or C113S) or Pin1 (W34A or K63A), with readings taken every 4 days. **** adj. $p < 0.0001$ by Bonferroni-corrected two-way ANOVA. For **f** and **h**, data points are plotted as the average of n = 3 biologically independent samples ± SEM, and are representative of n =

2 independent experiments. Uncropped immunoblots for **a**, **e**, and **g** are displayed in Supplementary Figure 12, and are representative of n = 2 independent experiments.

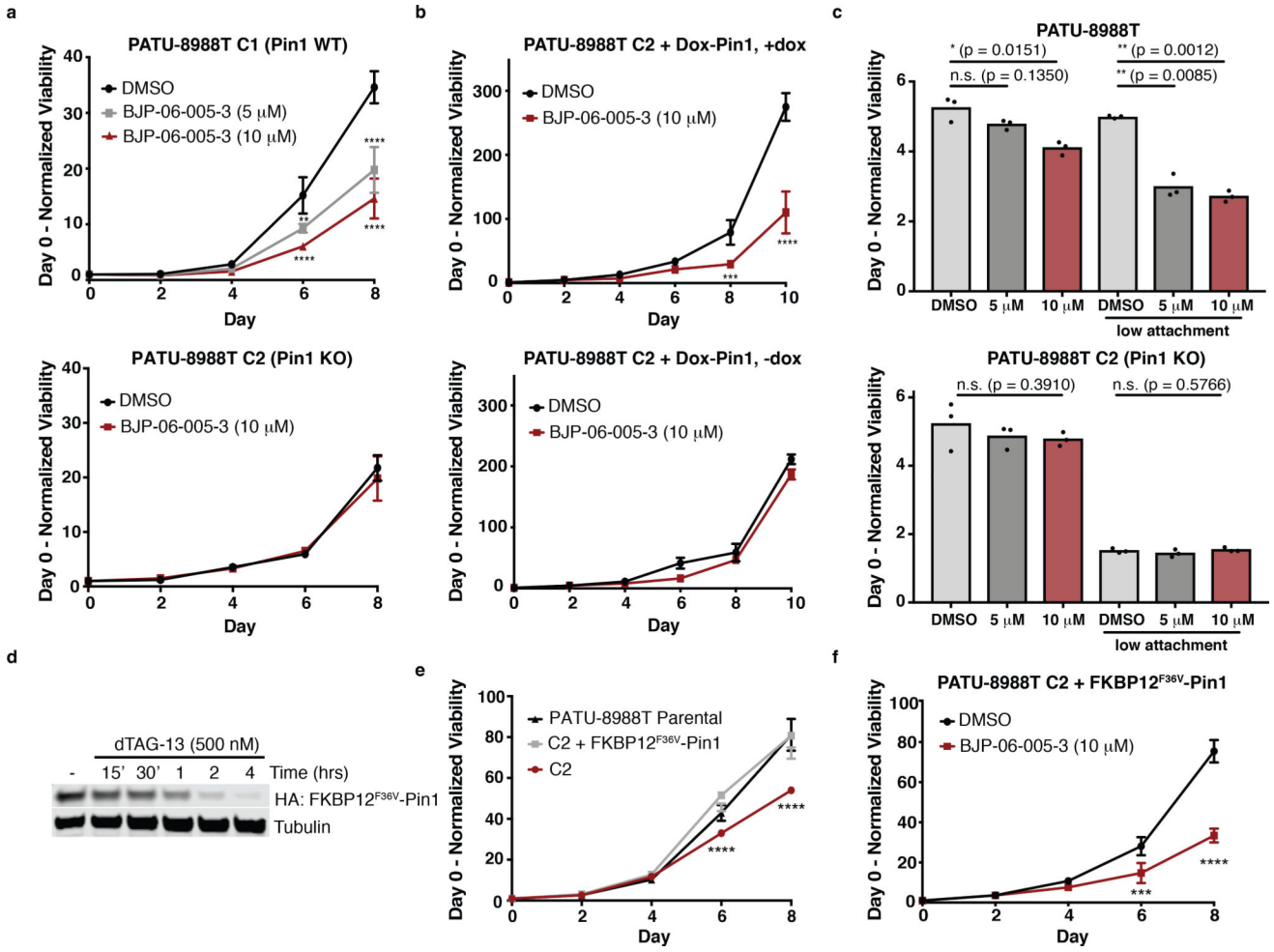

Figure 5 |. BJP-06–005-3 impacts PDAC cell viability in a Pin1-mediated manner.

(**a**) Day 0-normalized growth rate of C1 (above) or C2 (below), treated with DMSO or BJP-06–005-3 (5 or 10 μM), with readings taken every 2 days. ** adj. p = 0.0063, **** adj. p < 0.0001 by Bonferroni-corrected two-way ANOVA; (**b**) Day 0-normalized growth rate of C2 + Dox-inducible Pin1, treated with DMSO or BJP-06–005-3 (10 μM), in the presence (above) or absence (below) of Dox (100 ng/mL), with readings taken every 2 days. *** adj. p = 0.0005, **** adj. p < 0.0001 by Bonferroni-corrected two-way ANOVA; (**c**) PATU-8988T cells (parental: above; C2: below) were cultured in 2D-monolayers or as 3D-spheroids (indicated by "low attachment") and treated with DMSO or BJP-06–005-3 (5 or 10 μM) for 4 days, with compound re-treatment on day 2. The mean peak height of n = 3 biologically independent samples are shown as dot-plots, and are representative of n = 2 independent experiments. P values were derived from Welch's two-sided t-test, with comparisons made to DMSO. n.s. = not significant; (**d**) Immunoblot analysis of C2 + FKBP12^{F36V}-Pin1 cells treated with dTAG-13 (500 nM) for the indicated time points. Uncropped immunoblots are displayed in Supplementary Figure 12, and are representative of n = 3 independent experiments; (**e**) Day 0-normalized growth rate of PATU-8988T parental, C2, and C2 + FKBP12^{F36V}-Pin1, with readings taken every 2 days. **** adj. p < 0.0001 by Bonferroni-corrected two-way ANOVA; (**f**) Day 0-normalized growth rate of C2

+ FKBP12^{F36V}-Pin1 cells treated with BJP-06–005-3 (10 μM), with readings taken every 2 days. *** adj. p = 0.0001, **** adj. p < 0.0001 by Bonferroni-corrected two-way ANOVA. For **a**, **b**, **e**, and **f** data points are plotted as the average of n = 3 biologically independent samples ± SEM, and are representative of n = 3 independent experiments.

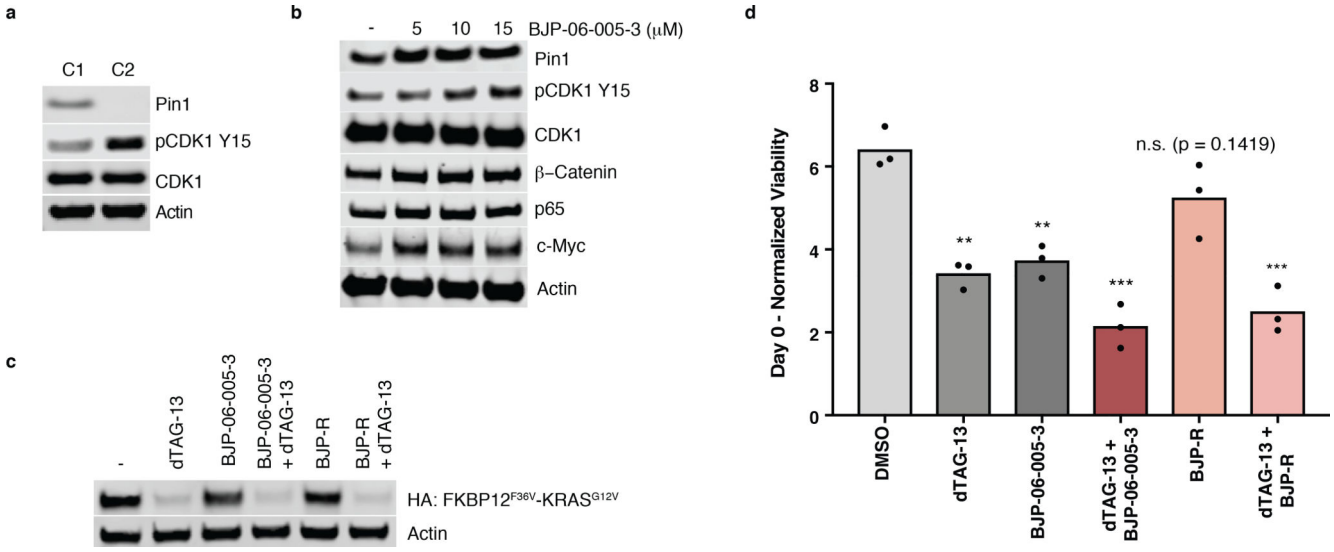

Figure 6 |. BJP-06–005-3 affects expression of downstream Pin1 substrates, and cooperates with KRAS^{G12V} degradation.

(**a**) Immunoblot analysis of lysates from C1 and C2; (**b**) Immunoblot analysis following BJP-06–005-3 treatment at the indicated concentrations for 5 h in C1; (**c**) Immunoblot analysis of PATU-8988T FKBP12^{F36V}-KRAS^{G12V}; *KRAS*$^{-/-}$ clone treated with dTAG-13 (100 nM), BJP-06–005-3 (5 μM), BJP-R (5 μM), or the indicated combinations for 4 h; (**d**) Day 0-normalized viability of PATU-8988T FKBP12^{F36V}-KRAS^{G12V}; *KRAS*$^{-/-}$ clone treated with dTAG-13 (100 nM), BJP-06–005-3 (5 μM), BJP-R (5 μM), or the indicated combinations for 4 days, with compound replenishment on day 2. The mean peak height of n = 3 biologically independent samples are shown as dot-plots, and are representative of n = 3 independent experiments. dTAG-13 ** p = 0.0017, BJP-06–005-3 ** p = 0.0022, dTAG-13 + BJP-06–005-3 *** p = 0.0005, dTAG-13 + BJP-R *** p = 0.0009 by Welch's two-sided t-test, with comparisons made to DMSO. n.s. = not significant. Uncropped immunoblots for **a** are displayed in Supplementary Figure 12 and are representative of n = 2 independent experiments. Uncropped immunoblots for **b** are displayed in Supplementary Figure 13, and are representative of n = 3 independent experiments. Uncropped immunoblots for **c** are displayed in Supplementary Figure 13, and are representative of n = 2 independent experiments.